Ion microprobe measured stable isotope evidence for ammonite habitat and life mode during early ontogeny

Benjamin J. Linzmeier, Neil H. Landman, Shanan E. Peters, Reinhard Kozdon, Kouki Kitajima, and John W. Valley

Abstract.—Ammonites have disparate adult morphologies indicative of diverse ecological niches, but ammonite hatchlings are small (~1 mm diameter), which raises questions about the similarity of egg incubation and hatchling life mode in ammonites. Modern *Nautilus* is sometimes used as a model organism for understanding ammonites, but despite their outward similarities, the groups are only distantly related. Trends in ammonite diversity and extinction vulnerability in the fossil record contrast starkly with those of nautilids, and embryonic shells from Late Cretaceous ammonites are two orders of magnitude smaller than nautilid embryonic shells. To investigate possible environmental changes experienced by ammonite hatchlings, we used secondary ion mass spectrometry (SIMS) to analyze the oxygen and carbon isotope composition of the embryonic shells and early postembryonic whorls of five juveniles of *Hoploscaphites comprimus* obtained from a single concretion in the Fox Hills Formation of South Dakota. Co-occurring bivalves and diagenetic calcite were also analyzed to provide a benthic baseline for comparison. The oxygen isotope ratios of embryonic shells are more like those of benthic bivalves, suggesting that ammonite eggs were laid on the bottom. Ammonite shell immediately after hatching has more negative $\delta^{18}O$, suggesting movement to more shallow water that is potentially warmer and/or fresher. After approximately one whorl of postembryonic growth, the values of $\delta^{18}O$ become more positive in three of the five individuals, suggesting that these animals transitioned to a more demersal mode of life. Two other individuals transition to even lower $\delta^{18}O$ values that could suggest movement to nearshore brackish water. These data suggest that ammonites, like many modern coleoids, may have spawned at different times of the year. Because scaphites were one of the short-term K-Pg survivors, it is possible that this characteristic allowed them to develop a broader geographic range and, consequently, a greater resistance to extinction.

Benjamin J. Linzmeier. Department of Earth and Planetary Sciences, Northwestern University, Evanston 60208, Illinois, USA, and Department of Geoscience, University of Wisconsin-Madison, Madison 53703, Wisconsin, USA. Email: benl@earth.northwestern.edu. Neil H. Landman. Division of Paleontology, American Museum of Natural History, New York 10024, New York, USA. Shanan E. Peters. Department of Geoscience, University of Wisconsin-Madison, Madison 53703, Wisconsin, USA. Reinhard Kozdon. Lamont-Doherty Earth Observatory, Columbia University, Palisades 10964, New York, USA, and WiscSIMS, Department of Geoscience, University of Wisconsin-Madison, Madison 53703, Wisconsin, USA. Kouki Kitajima and John W. Valley. Department of Geoscience, University of Wisconsin-Madison, Madison 53703, Wisconsin, USA and WiscSIMS, Department of Geoscience, University of Wisconsin-Madison, Madison 53703, Wisconsin, USA.

Data available from the Dryad Digital Repository: https://doi.org/10.5061/dryad.pq70h50 .

Introduction

The life history traits of extinct organisms are difficult to determine but such traits may influence extinction selectivity. Across the Cretaceous/Paleogene (K/Pg) boundary, evidence supports selection by characteristics including geographic range (Jablonski and Hunt 2006; Payne and Finnegan 2007; Landman et al. 2014), physiology (Knoll et al. 2007), and larval ecology (Jablonski and Hunt 2006). Among the victims of the K/Pg extinction are the ammonites, and their early life history has been the subject of much interest (Ward and Bandel 1987; Ritterbush et al. 2014; De Baets et al. 2015). The egg size and hatchling ecology of ammonites contrasts strongly with that of the co-occurring nautilids at the K/Pg boundary, a condition that was established and persisted since the Late Devonian (Wani 2011; De Baets et al. 2012). Identifying the presence or absence of a planktic stage, meaning shallow-water habitat and not explicitly passive floatation (i.e., not on bottom), in ammonites at the K/Pg understanding the habitat is important because that stage may have been vulnerable during ocean acidification (Arkhipkin and Laptikhovsky 2012).

No general consensus exists about the development depth or habitat of ammonite eggs (Ritterbush et al. 2014; De Baets et al. 2015). Some authors have proposed ovoviviparity or brooding (Ward and Bandel 1987; Jacobs and Chamberlain 1996), based on the preservation of eggs within adult body chambers (Mironenko and Rogov 2015) or modification to the adult body chamber that could contain eggs (Landman 1987). Others have suggested independently floating egg masses because of preservation in association with planktic gastropods and rare benthic organisms (Mapes and Nützel 2009) or egg masses attached to floating debris (Westermann 1996). Putative ammonite eggs from the Jurassic have been inferred to suggest benthic deposition (Etches et al. 2009). In modern octopods, adult depth habitat and hatching living

depth are not predictable from egg size (Boletzky 1978), so it seems unlikely that all ammonites had a similar egg development pathway (De Baets et al. 2015).

Many ammonite hatchlings were likely planktic (i.e. free floating, poorly-swimming, shallow water dwelling, Ritterbush et al. 2014; De Baets et al. 2015), however some authors suggested sessile benthic or suspended sessile lifestyles (Stinnesbeck et al. 2016). Several lines of indirect evidence suggest that hatchling ammonites could be planktic. Their small size, generally between 0.5 and 1 mm suggests a planktic stage due to similar sizes in modern planktic cephalopods (Landman 1987; Wani 2011). However, because there are no closely related modern analogs for ammonite ecology, it is possible that hatchling size and ecology in ammonites had a different relationship than that of modern coleoids (Jacobs and Landman 1993; Kröger et al. 2011). Other authors have suggested that accumulations of newly hatched ammonites in facies that suggest anoxic bottom waters where eggs could not survive point to planktic hatchlings (Mapes and Nützel 2009; De Baets et al. 2012). Shells may be transported into locations with anoxic bottom waters, or intermittent anoxia could produce similar patterns (Stephen et al. 2012). Buoyancy calculations from shells suggest neutral to positive buoyancy at hatching (Shigeta, 1993; Westermann, 1996; Lemanis et al., 2015). To calculate buoyancy, soft tissue density and morphology must be assumed because ammonite soft tissue has minimal preservation (Klug et al. 2012), potentially due to a persistent preservation bias caused by ammonia in the soft tissues (Clements et al. 2017).

If some or all ammonite hatchlings and eggs were planktic, then there must have been a transition to a demersal mode of life in at least some groups. The comparison of stable isotope ratios in ammonites to co-occurring sessile benthic organisms suggests some adults were demersal, free-swimming near the seafloor (Moriya et al. 2003; Moriya 2015; Sessa et al. 2015). Fully mature adult scaphites were likely demersal, a conclusion supported by considerations

89 from shell geometry and stable isotope evidence (Landman et al. 2012*a*; Sessa et al. 2015). The
90 neanoconch stage is proposed to be the transition between the planktic and demersal modes. This
91 stage is thought to occur at a diameter of 3-5 mm and is expressed by minor changes in shell
92 morphology and the appearance of ornamentation (Landman 1987; Westermann 1996).
93 Habitat change can be interpreted from the isotopic expression of environmental
94 gradients recorded in the shells of organisms that lived in the same environment or passed
95 through it. In a stratified water mass, the thermocline and the biological pump influence $\delta^{18}O$ and
96 $\delta^{13}C$ respectively. The biological pump refers to photosynthesis that preferentially removes low-
97 $\delta^{13}C$ carbon from the surface water and then degradation of organic matter in the bottom waters
98 releasing low $\delta^{13}C$ carbon (e.g. Kroopnick et al. 1972; Hain et al. 2014). Ammonites are thought
99 to precipitate their shell in oxygen isotopic equilibrium with seawater in analogy with modern
100 *Nautilus* (Cochran et al. 2003; Moriya et al. 2003; Zakharov et al. 2006; Lukeneder et al. 2010;
101 Kruta et al. 2014; Stevens et al. 2015; Linzmeier et al. 2016). Habitat change through ontogeny
102 has been inferred from serial $\delta^{18}O$ aragonite ($\delta^{18}O_{arag}$) sampling of the septa and shell wall in
103 larger specimens (Fatherree et al. 1998; Lukeneder et al. 2010; Zakharov et al. 2011; Lukeneder
104 2015; Stevens et al. 2015). However, sample mass requirements of micromill sampled traditional
105 phosphoric acid isotope analyses have prevented analysis of the earliest whorls of ammonite
106 shells, where the shell wall is <50 μm thick. Sampling ~10-μm diameter spots for $\delta^{18}O$ and ~7-
107 μm spots for $\delta^{13}C$ is possible by using secondary ion mass spectrometry (SIMS) and allows *in*
108 *situ* analysis of volumes many orders of magnitude smaller than traditional techniques.
109 In this study, we compare high-spatial resolution, high-analytical precision stable isotope
110 sampling of well-preserved ammonites and co-occurring bivalves and surrounding diagenetic
111 calcite from the upper Maastrichtian of the U.S. Western Interior to determine the habitat in
112 which the eggs and hatchlings developed. We show how these results contrast with previously

published data on habitat change of newly hatched nautilids and broadly discuss the implications of our data for understanding the dynamic epeiric seaway paleoenvironment and the K/Pg extinction.

Geologic Background

The specimens used in this study are attributed to the late Maastrichtian ammonite *Hoploscaphites comprimus*. They were collected from the Upper Cretaceous (upper Maastrichtian) Fox Hills Formation of south-central South Dakota (Fig. 1) and are housed at the American Museum of Natural History in New York City (Sample number = AMNH number: J-125 = 85630, J-145 = 85629, J-209 = 85613, J-215 = 85632, J-273 = 75647). The Fox Hills Formation constitutes the marginal marine phase of a progradational sequence deposited during the final retreat of the Western Interior Seaway (WIS). At its maximum extent, this seaway extended from the western Canadian Arctic to the proto-Gulf of Mexico (Gill and Cobban 1966). In the early part of the late Maastrichtian, the shoreline of the WIS cut across the western half of South Dakota and formed a broad delta (the Sheridan Delta) at the southeastern corner of Montana and the northeastern corner of Wyoming (Cobban et al. 1994; Landman et al. 2013). The exact temperature, magnitude, and seasonal duration of stratification in the WIS is unknown (Kump and Slingerland 1999; Petersen et al. 2016). However, stable isotope evidence from biogenic carbonates suggests that water column stratification occurred at least episodically (Tsujita and Westermann 1998; Fisher and Arthur 2002; Petersen et al. 2016).

To limit confounding factors of long-term climate change on the interpretation of the oxygen isotope results, we focused on five specimens from a single concretion. The ammonites are from the so-called *abyssinus* or transition concretions at the contact between the underlying Trail City Member and the overlying Timber Lake Member of the Fox Hills Formation (Landman and Waage, 1993, Fig. 2). These concretions occur in or just below the *Sphenodiscus*

Layer. The locality is in the southwest facing exposures on the ridge extending northwest from bluffs on the Timber Lake Member, about 4 km west-southwest of Green Grass (Fig. 1, NE1/4SE1/4 sec. 21, T. 14N., R. 23E., Lantry NE quadrangle, Dewey County, South Dakota 45.16041N, -101.306W). This locality was positioned approximately 75 km east of the paleoshoreline, but the exact position relative to the coast is difficult to pinpoint and the coast itself likely consisted of extensive wetlands and numerous embayments (Landman et al. 2013). These concretions contain abundant juvenile ammonites and plant material. They are interpreted to have been deposited on the lower shore face or transition zone (Landman and Waage 1993).

Material

The transition concretions contain numerous small juvenile ammonites. These specimens are assigned with confidence to *H. comprimus* based on several criteria. Even though they are juveniles, they are identical in terms of their shell shape and ornamentation to the early whorls of this species. Landman and Waage (1993: Fig. 81) dissected adults of *H. comprimus* to reveal the change in characters through ontogeny. The juvenile shell bears fine growth lines that parallel the ornamentation. Ribs first appear at approximately 4-5 mm in shell diameter and cross the venter with a marked forward projection. Primary ribs are straight to slightly sinuous and rectiradiate to prorsiradiate. Specimens of *H. comprimus* are consistently more compressed through ontogeny than those of the biostratigraphically older species *H. nicolletii*. In addition to the similarity of the morphology between the juveniles that are present in the concretion and the dissected early whorls of *H. comprimus*, the few adult ammonites that occur in these concretions also belong to the same species. We analyzed five juveniles (informal numbers: J-125, J-145, J-209, J-215, and J-273) that we attribute to *H. comprimus*.

All of the individuals sampled in this study consist of the phragmocone filled with calcite and part of the body chamber filled with detrital sediment (Fig. 3, Fig. 4, and Fig. 5). They are

2.9-7.8 mm in diameter (1.7-4.9 mm in phragmocone diameter), with a little more than two whorls growth beyond of the primary constriction (Fig. 3 and Fig. 5 A). The angle of the body chamber ranges from 178 to 230º. J-125 is 6.5 mm in diameter and is wholly septate. We used SIMS to analyze fragments of three specimens of bivalves with calcitic shells and the diagenetic calcite spar infilling the ammonite chambers (Fig. 6). Bivalves are benthic mollusks that have either an epifaunal or infaunal mode of life and therefore record the temperature and water conditions on or in the upper few centimeters of the sediment. Diagenetic calcite preserves pore fluid conditions during precipitation. Two additional whole bivalves were sampled by micromill (Fig. 6). The whole bivalves are *Protocardia*, but the fragments, analyzed by SIMS, are unidentifiable, probably either *Protocardia* or *Tenuipteria* as whole individuals of these genera are also present in the J concretion (Speden 1970). Because these fragments appear to be from different species and still exhibit similar $\delta^{18}O$ values, strong vital effects seem unlikely. Although the bivalves and the ammonites sampled here may not have lived in the exact same environment, bivalve results may record regional seawater characteristics (Sessa et al. 2012).

Terminology

Embryonic scaphite shells are composed of aragonite and consist of the protoconch and approximately two-thirds of the first whorl (Fig. 7). Collectively the embryonic shell is known as the ammonitella. The embryonic shell terminates in the primary constriction and associated varix and is approximately 700 μm in diameter (Landman et al. 1996). The outer shell wall of the embryonic shell is prismatic except for the primary varix, which is nacreous (Landman et al. 1996). The outer shell wall of the postembryonic shell consists of an outer prismatic and inner nacreous layer. The boundary between the two layers, an organic rich membrane may be phosphatized (Tanabe et al. 2012).

Methods

Samples were mechanically removed from the J Concretion, mounted in epoxy (Buehler EpoKwik), and then subsequently ground to the medial plane. Excess initial epoxy was cut away and later shells were recast in Buehler Epoxide Resin QT and Epoxide Hardener (6:1 epoxy to hardener by mass) with calcite standard UWC-3 ($\delta^{18}O$ = 12.49‰, Vienna Standard Mean Ocean Water (VSMOW) or -17.87‰ Vienna Pee Dee Beleemnite (VPDB); $\delta^{13}C$ = -0.91‰ (VPDB) Kozdon et al. 2009). Samples were ground and polished to eliminate surface relief to minimize variability of instrumental bias and enhance reproducibility (Kita et al. 2009).

We assessed diagenesis of the shell by scanning electron microscopy (SEM) using energy dispersive spectroscopy (EDS), backscattered electron (BSE) imaging and electron backscatter diffraction (EBSD) detectors. EBSD was used to determine mineralogy as an additional test for diagenesis because aragonite readily alters to calcite (Cusack et al. 2008). The composition of the outer shell was confirmed to be aragonite. BSE imaging revealed the nacreous and prismatic microstructure indicating the original shell preservation (Fig. 5 B and C, Cochran et al. 2003). Within instrumental detection limits (20 second live time, 15 kV), EDS indicated that minor element composition was different enough between materials sampled by SIMS to induce different instrumental mass fractionation between the diagenetic calcite and bivalve calcite (UWC-3 calcite standard wt %: Mn ~0.1, Mg ~0.5, Fe ~0.4 (Kozdon et al. 2009), Ammonite wt %: Mn ~0.5, Mg ~0.1, Fe 0.0, Bivalve Calcite wt %: Mn ~0.0, Mg ~0.1, Fe ~0.4, Diagenetic Calcite wt %: Mn ~3.2, Mg ~1.8, Fe ~1.4). This could adjust the $\delta^{18}O$ of diagenetic calcite by approximately -1.7‰ and would align our measured values with the bivalve calcite but would not alter our interpretations of the measurements in the ammonites. Locations for SIMS analysis on the ammonite shells were selected based on shell preservation and amount of change in $\delta^{18}O$ from adjacent pits during the analysis session.

SIMS Analysis

Oxygen and carbon isotope analyses were performed using a CAMECA IMS-1280 ion microprobe at WiscSIMS (Wisconsin Secondary Ion Mass Spectrometer Laboratory), UW-Madison (Kita et al. 2009; Valley and Kita 2009). After analysis the sample surface was reimaged and both images and SIMS pit data were combined in QGIS (QGIS.org) following the procedures outlined in Linzmeier et al. (2018). Most $\delta^{18}O$ analyses were from spots 10-µm in diameter (Samples n = 475, Standards n = 235); additional analyses with 3-µm spots (Samples n = 41, Standards n = 52, Fig. 5 C) were performed to sample either the prismatic or nacreous layers in locations where larger spots could not cleanly sample only one layer. Spot size can vary by 10%. Most 10-µm analyses are of the outer shell (n = 418), including 158 analyses that are clearly placed in the nacreous layer, 68 spots that are clearly positioned in the prismatic layer, and multiple mixed measurements (n = 83), but several analyses are of the later septa (n = 9). Some analyses minimally intersected diagenetic calcite and are placed either in the nacreous layer (n = 31), the prismatic layer (n = 30), or both (n = 48). Carbon isotope analyses were done with a 7-µm beam diameter (Samples n = 154, Standards n = 92). Raw and instrumental mass fractionation corrected oxygen and carbon isotope ratios measured on the five ammonite specimens (J-125, J-145, J-209, J-215 and J-273) are available in separate supplementary data tables (SI 6 and 7). A series of reflected light maps and SEM images of pits are also included in the supplementary information (SI 1 to SI 5).

Four analyses of the UWC-3 standard were made before and after each set of 10–15 sample measurements. At the start of each session the instrumental bias between calcite and aragonite was calibrated with analysis of UW-Arg-7, aragonite standard ($\delta^{18}O$ = 19.73 ‰, VSMOW, $\delta^{13}C$ 5.99‰, Orland 2012; Linzmeier et al. 2016). Standards bracketing analyses on samples were used to calculate the instrumental bias in order to correct measured $\delta^{18}O$ and $\delta^{13}C$ values to the Vienna Pee Dee Belemnite (VPDB) scale (Kita et al. 2009) as well as to evaluate

233 the external reproducibility of the measurements. For all analyses, either $^{16}O^{1}H$ or $^{13}C^{1}H$ was
234 measured simultaneously with the stable isotope ratio and $^{16}O^{1}H/^{16}O$ (OH/O) or $^{13}C^{1}H/^{13}C$
235 (CH/C) are interpreted to track intra-sample organic or water components (Linzmeier et al.
236 2016). The spot-to-spot reproducibility or external precision of each set of bracketing standards
237 for $\delta^{18}O$ averaged ~0.3‰ (2 SD) for 10-µm spots, ~0.8‰ (2 SD) for 3-µm spots and ~0.7‰ (2
238 SD) for $\delta^{13}C$ analyses. Detailed descriptions of the analytical conditions and the instrument setup
239 have been published previously (Orland et al. 2009; Kozdon et al. 2013; Vetter et al. 2014;
240 Linzmeier et al. 2016; Śliwiński et al. 2016*a*, *b*). SIMS spots were initially selected based on
241 reflected light, SE, and BSE images taken before analysis. After analysis, spots were classified
242 based on the material sampled by each pit as identified in SE images. Pits including even a minor
243 amount of diagenetic calcite were conservatively classed as including diagenetic calcite. During
244 analysis, if an area showed detectable change between two points, additional pits were placed
245 between them. Exclusion of pits based on low ion yield, high OH/O, high CH/C, or intersection
246 with diagenetic calcite does not change our conclusions.

247 Some disagreement in oxygen isotope values between SIMS and the phosphoric acid
248 digestion technique has been observed in Recent (<100,000 years) biogenic calcite and
249 speleothems (Rollion-Bard et al. 2007; Aubert et al. 2012; Orland et al. 2015*a*, *b*; Wycech et al.
250 2018). Oxygen isotope ratios measured by phosphoric acid digestion technique also may vary
251 with pretreatment (Wierzbowski 2007; Tobin et al. 2011). The magnitude of the offset is
252 systematic for similar samples and OH/O, we observe the offset to be constant and less for older
253 samples (Orland et al. 2015*b*). Thus, because our samples are Cretaceous in age and the patterns
254 and ranges of values within samples are critical to interpreting life history, a systematic offset
255 would not affect the $\delta^{18}O$ proxy for relative position in the water column. Unless an instrumental
256 offset exists that is different between the bivalves and ammonites, our interpretations of relative

position in the water column should be robust, however absolute temperature estimates may be biased toward warmer values.

Micromilling and Bulk Isotope Analysis

Two whole bivalves were serially sampled using a dental burr made of carbide in a hand-held microdrill to complement the datasets collected on bivalve fragments by SIMS (Fig. 6). Shallow trenches were made in the shell parallel to growth banding (Fig. 6). Powdered shell was then sent to Isolab at the University of Washington, where $\delta^{13}C$ and $\delta^{18}O$ of carbonate were measured using a Finnigan Delta Plus mass spectrometer with attached Kiel III Carbonate Device (SI 8). Carbonate was reacted with five drops of phosphoric acid at 70°C for ten minutes. Measured values were converted to the VPDB scale by standardization with calcite reference materials (NBS – 18 and NBS – 19) and using the calcite acid fractionation factor published by (Kim et al. 2007*a*). External precision of analyses were 0.07‰ (2 sd) for $\delta^{18}O$ and 0.16 ‰ (2 sd) for $\delta^{13}C$.

Synthetic Aragonite Comparison

Comparing isotope ratios measured in calcite to those measured in aragonite across both methods requires an adjustment to account for the difference in isotope ratio between the minerals during equilibrium preciptiation. The adjustment to synthetic aragonite from measured calcite isotope ratios was performed using fractionations from Romanek et al. (1992, +1.7‰ $\Delta^{13}C_{aragonite\text{-}calcite}$ from 0 to 40 °C) and (Kim et al. 2007*b*) +0.8‰ $\Delta^{18}O_{aragonite\text{-}calcite}$ at 25 °C). For simplicity of comparison between mineral phases, all $\delta^{13}C$ and $\delta^{18}O$ ratios from calcite (bivalves and diagenetic calcite) are reported as the calculated value of equilibrated aragonite($\delta^{18}O_{AragCal}$ and $\delta^{13}C_{AragCal}$). Raw and corrected data are included in supplemental tables (SI 6 and 7).

Oxygen Isotope Temperature Calculation

Temperatures are calculated from measured $\delta^{18}O$ values assuming equilibrium precipitation with seawater. The aragonite-temperature equation of (Kim et al. 2007*b*) is used because of a wider temperature calibration (0 – 40 °C) of laboratory-precipitated inorganic aragonite compared to that of the commonly used calibration of Grossman and Ku (1986, 2.6 – 22.0 °C), that was determined using wild-collected aragonitic gastropod and scaphopod mollusks. Grossman and Ku (1986) and other biogenic aragonite derived temperature equations are statistically indistinguishable from the calibration of Kim et al. (2007*b*). The Kim et al. (2007*b*) equation is as follows:

$$1000ln\alpha_{aragonite.\ water} = 17.88 \pm 0.13\,6\frac{10^7}{T}\Big) - 31.14 \pm 0.46$$

We solve for temperatures assuming $\delta^{18}O_{water}$ = -1.0, -2.0, and -3.0 ‰ (VSMOW) because of the likely influence of brackish water on this environment (Dennis et al. 2013; Petersen et al. 2016; Whitney et al. 2017).

Data Analysis

Calculation of post-embryonic growth in whorl number (degrees) for each specimen was done in R (R Core Team 2017). A center point for each ammonite shell was determined and the angle between lines to the center of the shell was calculated. Change-point analysis was done to identify the locations of stepwise change in mean $\delta^{18}O$ and $\delta^{13}C$ values across the ammonite shells using a *cpt.mean* without penalty within the *changepoint* package for R (Killick and Eckley 2014). An analysis of variance (ANOVA) hypothesis test *aov* was done to determine if the mean $\delta^{18}O$ was equal across embryonic whorls, varix, and first two post-varix whorls using R. Pairwise contrasts for the equality of means were done for these groups using Tukey's honestly significant differences function *tukeyHSD* that corrects for increased likelihood of

rejecting the null hypothesis of no difference between groups. Tables of results for contrasts are included in the supplemental data (SI 11).

Results

Transition Concretions

The carbonate-cemented concretion in which the ammonites occur is small, approximately 40 cm in diameter, and contains small protobranch bivalves, abundant plant fragments (nuts), abundant juvenile scaphites, ammonite jaws, ammonite hook-like structures and rare adult scaphites (microconchs of *H. comprimus* and *H. nicolletii*). Both ammonite jaws and hook-like structures have not been found in body chambers. It contains approximately 326 juvenile specimens of *H. comprimus*. A histogram of the juvenile specimens reveals a mode between 4 and 6 mm (Fig. 8). The body chambers of the juveniles are commonly broken, although some attain a body chamber length of 270º. The concretion used in this study is similar to three other concretions analyzed from the same horizon that also contain an unusual abundance of juveniles and differs from other concretions in the Trail City Member (Fig. 8, Landman et al. 2008).

Shell Morphology

Several of the specimens exhibit varices or shell thickenings that are irregularly spaced (Table 1, Fig. 3 and Fig. 5 A). Some varices are associated with pockets of pyrite either inside of them or inside the adjacent chamber. Varices have not been documented before in *Hoploscaphites*. The presence of regularly spaced varices is diagnostic of the genus *Desmoscaphites* (Landman and Cobban 2007). Because the varices observed in these *Hoploscaphites* are irregularly spaced, they may be pathological and formed in response to an irritant or parasite (De Baets et al. 2011).

Oxygen Isotopes

Oxygen isotope ratios were sampled from diagenetic calcite, calcitic bivalves, and aragonitic ammonites (Fig. 9). Within diagenetic calcite in ammonite mounts, no major differences were observed in the $\delta^{18}O$. Differences of up to ~2‰ are detectable between ammonite mounts J-125 and J-273 and they bracket the range of values measured across all samples. The $\delta^{18}O_{AragCal}$ values of diagenetic calcite for all mounts average -0.6‰.

All bivalves have similar $\delta^{18}O$ values. The $\delta^{18}O_{Arag.Cal}$ measured by SIMS average -2‰ (VPDB). The average values for each bivalve by SIMS are -2.4‰ for J-273, -1.7‰ for J-215, and -2.1‰ for J-125. Average $\delta^{18}O_{AragCal}$ values for the two bivalves that were micromilled (DG and NG, Fig. 6 and Fig. 9) are -1.5‰ and -2.4‰ (VPDB).

Broad similarities exist in $\delta^{18}O$ across the sampled portions of the five ammonites. No differences in $\delta^{18}O$ were detected between adjacent nacreous and prismatic shell by either ~10 μm or ~3 μm analyses (Fig. 7, Fig. 10, and Fig. 11). Embryonic shell, precipitated before the varix and at the center of the shells, has a higher $\delta^{18}O$ value than that of the varix (Fig. 10, Table 2). These values on embryonic shell overlap with those of the bivalves and varix $\delta^{18}O$ is generally are lower than bivalve (Fig. 10). The isotope values in the immediate postembryonic whorls are the same or lighter than those at the varix (Fig. 10, Table 2). Change-points are detected in all five ammonites between 0.75 and 1.5 whorls post-varix (Fig. 10). Exclusion of data based on relative ion yield, measured $^{16}O^{1}H/^{16}O$, or intersection with negligible amounts of diagenetic calcite does not substantially change the observed patterns within or between ammonites.

Differences in the patterns of $\delta^{18}O$ though ontogeny were also observed. The embryonic, varix, and first two half-whorls post-varix do exhibit the same mean $\delta^{18}O$ within and across sample mounts (ANOVA, $p = <0.002$). Tukey's Honestly Significant difference test (Miller 1981) was done to test multiple contrasts at the 95% confidence level including testing grouped

embryonic whorls, varix, and first two half-whorls growth for equal means (6 contrasts per individual). The summary tables for these contrasts are included as SI 11. Average absolute values for the embryonic and varix measured $\delta^{18}O$ are significantly different in J-125, J-145, and J-209, but not J-215 and J-273 (Fig. 10, Table 2, SI 11). Average $\delta^{18}O$ in embryonic shell was significantly higher ($p < 0.01$) than that of the first whorl and the first whorl in all but specimen J-209 (Fig. 10, Table 2, SI 11). The direction and magnitude of $\delta^{18}O$ change at the detected change-points group broadly into two patterns, a stepped decrease (J-125, J-145, Fig. 10 A) and stepped increase (J-209, J-215, J-273, Fig. 10 A, B). In J-209, the $\delta^{18}O$ values from shell precipitated later than the varix varies with a greater magnitude than in the other ammonites, and sometimes match those of the bivalves.

Oxygen Isotope Temperatures.—

Seawater temperatures calculated from $\delta^{18}O$ measured in these ammonites range from ~16 to 35 °C if $\delta^{18}O$ of seawater ($\delta^{18}O_{SW}$) is assumed to be -1.0‰ (VSMOW), the commonly used value for seawater in an ice-free world (e.g., Shackelton and Kennett 1975) and the value determined from clumped isotope analysis of Fox Hills fossils (Dennis et al. 2013). Temperatures range from ~12 to 30 °C if $\delta^{18}O_{SW}$ was -2.0‰ (VSMOW) and ~8 to 25 °C if $\delta^{18}O_{SW}$ was -3.0‰ (VSMOW). The calculated temperature ranges within individuals are approximately 7 to 15 °C, assuming uniform $\delta^{18}O_{sw}$. Temperatures calculated for the average $\delta^{18}O$ per half whorl are summarized in Table 2.

Carbon Isotopes

Carbon isotope ratios were measured by SIMS in three ammonites, three associated bivalves and diagenetic calcite (Fig. 12). Diagenetic calcite was distinctly different between the three mounts. An average value of -23.0‰ (VPDB, n = 4) was measured in J-215, an average of

-16.8‰ (VPDB, n = 5) was measured in J-125 and the heaviest average of -8.4 ‰ (VPDB, n = 4) was measured in J-273.

Bivalve calcite was similar in $\delta^{13}C$ between J-125 and J-215. J-215 has an average value of +5.6‰ (VPDB, n=12) and J-125 has an average value of +5.1‰ (n = 5). The bivalve associated with J-273 has a very different $\delta^{13}C_{AragCal}$, with an average value of -12.3‰ (n = 10). The micromilled bivalves and those associated with ammonites J-125 and J-215 have $\delta^{13}C_{AragCal}$ values that are close to +5‰.

In all three ammonite specimens analyzed for $\delta^{13}C$ (J-125, J-215, and J-273), there is no apparent difference between adjacent measurements in different microstructure after hatching (Fig. 12). The $\delta^{13}C$ value averages approximately 5.0‰ in the embryonic shell and then transitions to lighter values in the varix, ranging from an average of 0.0 to 2.0‰. Measured $\delta^{13}C$ values are more variable both between and within individuals in shell adoral of the varix. In J-125, the values are much lighter, and average -4‰ whereas in J-215 and J-273, the values are only slightly lighter and average 0.0 and -1.0‰, respectively. The $\delta^{13}C$ values become lighter throughout sampled ontogeny in all the specimens (Fig. 12).

Discussion

Timescale of Isotope Record

The fossils in this single concretion likely represent time averaging on the order of months to decades. Presence of ammonite jaws and hook-like structures in these concretions, even outside of body chambers, suggests that the ammonites did not have a protracted period of exposure on the sea floor before burial (Wani 2007). Similar calcareous concretions from the WIS are estimated to have accumulated in 10-50 years because of the incorporation of jaws and lack of encrustation, although these are from more offshore sites in the Pierre Shale and contain a higher diversity of fauna and more adults (Landman and Klofak 2012). Low incidence of borings

in these individuals also suggests low seafloor residence time especially in areas with high sedimentation rates (Tomašových et al. 2017). However, if we assume that the accumulation is not time averaged beyond 100 years, it implies that the ammonites sampled here were lived at nearly the same time and experienced similar environmental conditions (e.g. seasonal temperature range, mean annual temperature, freshwater input).

The sparry calcite infilling the ammonites is authigenic carbonate that was likely precipitated rapidly. Calcite wedging between the nacreous and prismatic layers of the shell (Fig. 3 and Fig. 5 C) and calcite wedging between tablets of nacre (Fig. 3 and Fig. 4, J-273) suggest rapid calcite precipitation at low temperatures because fine grained aragonite tends to recrystallize to calcite or dissolve (Rude and Aller 1991; Macintyre and Reid 1995; Cherns and Wright 2000; Sessa et al. 2009). SEM imaging also shows calcite encasing individual tablets of nacre in some places where the shell is broken (See SI 1 to 5). The low $\delta^{13}C$ measured in the authigenic calcite suggests the carbon source was likely the decaying mollusk or plant organic matter in the volume of the concretion (Landman and Klofak 2012; Landman et al. 2015). An alternative source for the low $\delta^{13}C$ values in the authigenic calcite is fresh groundwater, carrying low $\delta^{13}C_{DIC}$ from decay of terrestrial organic matter, flushing through the sediments before compaction. Both carbon and strontium isotopes suggest groundwater interaction was an important component of WIS hydrology (Cochran et al. 2003). Some modern, nearshore calcite-siderite concretions formed within the last 50 years through a combination of increased sedimentation and tidal groundwater flushing (Allison and Pye 1994). It is notable that there is no indication of aragonite shell dissolution even though pH is expected to decrease during organic matter degradation (Walter et al. 1993).

To interpret the stable isotope data collected from the ammonites, the timescale of mollusk growth must be estimated. Sinusoidal patterns in bivalve calcite $\delta^{18}O$ are widely

421 interpreted to indicate seasonal temperature variability that serves as a chronometer of growth
422 (e.g. Killingley and Berger 1979; Jones 1983; Ivany et al. 2003). However, the range of $\delta^{18}O$
423 within ammonites that exhibit sinusoidal variability (e.g. ~2‰, Fatherree et al., 1998, or ~0.8‰
424 Lécuyer and Bucher, 2006) have been argued to be too large for seasonality as the primary cause
425 (Lukeneder 2015). Other authors have interpreted $\delta^{18}O$ variability preserved in belemnite rostra
426 as reflecting primarily seasonal changes (Urey et al. 1951; Dutton et al. 2007). Ammonites were
427 likely mobile both vertically and horizontally in their environment, which is expected to add
428 variability to the isotopic composition of their growing shells (Linzmeier et al. 2016). Sinusoidal
429 variability in ammonite $\delta^{18}O$ values can, therefore, only dubiously be interpreted as reflecting
430 seasonal patterns. In adult scaphites, sinusoidal variability, if present, may be interpretable as
431 seasonality because a high degree of morphological partitioning by facies suggests more limited
432 long-distance movement of mature individuals (Jacobs et al. 1994) and the morphology of the
433 aperture, especially in mature shells, suggests limited swimming capacity (Landman et al.
434 2012*a*). In juvenile scaphites, sinusoidal variation in measured stable isotope ratios could also
435 indicate seasonality, however because circumstantial evidence suggests at least a portion of
436 early, post-hatching life was spent in shallow water, variation is likely an integrated signal of
437 changes in the location within the environment, as well as seasonal environmental change.
438 The best available estimates of growth can come from analogies with modern coleoid
439 cephalopods. Modern cephalopod growth is highly temperature dependent. Thus, if the
440 ammonites studied here grew at different times of the year then regardless of their realized size,
441 they may have been different in age even if they reached the same diameter (Boletzky 1983;
442 Summers 1983). Development in *Sepia officinalis* can take from over 100 to 30 days depending
443 if the egg grew in 15 or 25 °C water (Boletzky 1983). Food availability and temperature also

444 modulate the rate of statolith (internal biomineral) growth (Zumholz et al. 2006; Aguiar et al.
445 2012).

446 Because the ammonites studied here are small (< 8 mm), their growth rate (i.e. % mass,
447 diameter) was probably the most rapid of their lifespan. The evacuation of fluids from newly
448 formed chambers by osmosis through the siphuncle would have been fastest at small shell
449 volumes (Bucher et al. 1996). The rate of growth and age at maturity of *H. comprimus* is difficult
450 to determine because ammonites are all extinct. The total lifespan of *Hoploscaphites* is estimated
451 to be less than 6 years (Landman et al. 2012*a*). Data on modern cephalopods provide a context
452 for comparison. Growth rate estimates of modern cephalopods fall into two groupings. *Nautilus*
453 grows slowly and reaches maturity in 10-15 years (Landman and Cochran 2010). Shallow water
454 coleoids, such as *Loligo*, on the other hand grow quickly and reach maturity in 1 or 2 years
455 (Forsythe and Van Heukelem 1987). Jacobs and Landman (1993) have argued that ammonites
456 are phylogenetically closer to coleoids than to nautilids, implying that ammonites and coleoids
457 may have shared similar growth rates. However, the plesiomorphous retention of an external
458 shell must have imposed physiological constraints on the rate of growth. In addition, within the
459 ammonites themselves, growth rates probably varied widely depending on the depth of the
460 habitat, ranging from rapid rates in shallow water forms such as scaphitids to slower rates in
461 deeper water forms such as desmoceratids. On this basis, we estimate that the age of maturity of
462 *H. comprimus* is 3-5 years. This estimate is comparable to estimates of other shallow water
463 ammonites based on a variety of proxies including septal spacing, jaw increments, size classes,
464 and epizoans (Bucher et al. 1996).

465 Therefore, the isotope record from within the ammonites probably reflects weeks or
466 months, although not necessarily in the same year. Thus, in the ontogeny of any individual, the
467 data do not show complete annual temperature change, nor do they reflect long-term global

temperature change and the results should be interpreted considering sub-annual water mass conditions. This means that abrupt changes in isotope ratios probably reflect spatially close changes in the environment because the small scaphites are unlikely to have been fast swimmers with high mobility. Swimming velocity estimates suggest hatchling ammonites may have moved as much as ~167 m/day in calm water and jetting was likely important for maintaining position in the water column (Lemanis et al. 2015). Movement vertically in the water column could cause abrupt changes in temperature or salinity in the WIS (Petersen et al. 2016). Horizontal movement of water masses could also have occurred, but these would have likely developed over more time. Alternatively, the ammonites may have experienced changes as passive inhabitants being moved along the shoreline parallel to longshore current (Waage 1968).

Bivalve Interpretation

Seasonality or Partial Seasonality.—

Bivalve isotope data provide constraints on benthic temperature and seasonality characteristics in the WIS. Stable isotope data from bivalves in this study come from small fragmentary samples and therefore likely do not capture the full range of seasonal variability within any one individual (Fig. 6 and Fig. 9). Common sclerochronological estimation of seasonal range from sinusoidal fits cannot be done with this dataset because we have not found complete sinusoids (Ivany 2012). Potential seasonal magnitude, however can be conservatively estimated by the range in $\delta^{18}O$ within individuals capturing only partial years, which in this case averages 1.2‰ or ~5 °C. Pooling all data (SIMS and acid digestion) suggests a larger seasonal range of 3.7 ‰ or ~18°C, but potentially introduces confounding factors associated with transport from nearshore brackish water with different mean $\delta^{18}O$ or with species specific vital effects (Landman and Klofak 2012).

Bivalve $\delta^{13}C$ range – Infaunal Life or Transport? .—

A large $\delta^{13}C$ range (~22‰) was measured across bivalves in this concretion. Bivalve $\delta^{13}C$ reflects a combination of dietary and DIC sources (McConnaughey and Gillikin 2008). Most (4 of 5) have $\delta^{13}C$ values near +5‰ VPDB. These values are similar to the embryonic ammonite shells and may indicate an epifaunal or shallow infaunal mode of life and growth in the same water as the ammonites, because of large $\delta^{13}C_{DIC}$ gradients in porewaters (McCorkle et al. 1985). One bivalve has low $\delta^{13}C$ values that suggests either transport from more brackish water with lower $\delta^{13}C_{DIC}$ like similarly aged bivalves from the Hell Creek Formation (Cochran et al. 2003) or a deep infaunal mode of life across a $\delta^{13}C$ gradient within the sediment porewater (McCorkle et al. 1985). Similar changes in $\delta^{13}C$ are found in modern benthic foraminifera that live farther below the sediment water interface (McCorkle et al. 1997). Living near seeping methane can also drive $\delta^{13}C$ of mollusk carbonate low (Hein et al. 2006). However, well-developed seeps have not been identified in the Fox Hills (Landman et al. 2012*b*).

Ammonite Interpretation

Oxygen Isotopes.—

The isotope values of the embryonic shell provide insight into the environment in which the eggs developed (Landman et al. 1994). The fact that the $\delta^{18}O$ values of the embryonic shells approach those of the bivalves suggests that the eggs developed on the bottom (Fig. 10, Moriya et al. 2003; Zakharov et al. 2006; Sessa et al. 2015). A variety of modes of egg development have been proposed with benthic development including individual or masses of eggs deposited on the sea floor (Ritterbush et al. 2014; De Baets et al. 2015). A recent report of embryonic shells with *in situ* aptychi preserved in the body chamber of adults suggests ovoviviparity may have occurred in some ammonites (Mironenko and Rogov 2015). However, similar preservation has not been observed for scaphites. Most studies of the mode of life of scaphites suggest they lived in the bottom of the water column, therefore agreement between bivalve and embryonic

ammonite shell suggests ovoviviparity cannot be excluded (Landman et al. 2012*a*; Sessa et al. 2015). Future work may find females with developing embryos in the body chamber.

The average $\delta^{18}O$ for the embryonic shell is different between individuals (Fig. 10, Table 2), which may indicate that the eggs developed in different seasons. Some modern coleoids have protracted spawning seasons that span several months suggesting that this behavior is possible in ammonites (Worms 1983; Rocha and Guerra 1996; Rocha et al. 2001). The measured range in just the embryonic shell, combining all observations, would translate to a seasonal temperature range of ~8 ºC, which is comparable to the ranges observed within individual bivalves. However, the measured oxygen isotope ratio of J-215 and J-273 that approach -4‰ (VPDB) are unusually light. Temperatures for the two would be anomalously high at 31ºC ($\delta^{18}O_{SW}$ = -1.0‰) which suggests that they may also have developed at a different site, nearer to shore in slightly more brackish water, with a lower value of $\delta^{18}O_{SW}$.

The values of $\delta^{18}O$ consistently decrease from the embryonic shell into the varix by 0.6 to 1.1‰. This transition translates to an increase in temperature of approximately 4ºC. Data from post-hatching shell does not indicate a difference in $\delta^{18}O$ of adjacent nacreous or prismatic aragonite, so this transition can be interpreted as environmental change (Figs. 5, 9, and 10). The varix is thought to have developed during late embryogenesis (De Baets et al. 2015). It is also possible that the varix formed immediately before and immediately after hatching, reflecting the initial post-hatching environment. This change in $\delta^{18}O$ between embryonic shell and varix could reflect vertical movement in the water column to warmer or more brackish water at hatching, a scenario that is possible given buoyancy calculations and jetting potential (Lemanis et al. 2015). If brooding is considered as a possibility, the lighter values of both $\delta^{18}O$ and $\delta^{13}C$ in all five specimens may imply that the females migrated inshore at the end of embryonic development. The lighter values of $\delta^{18}O$ at the varix could also reflect hatching at a warmer time of the year or

seasons with lower $\delta^{18}O$ of seawater. Most of the specimens lack a sufficient number of data points in the embryonic shell to reveal a trend, but J-273 shows a partial sinusoidal pattern in $\delta^{18}O$ with a shift toward warming near the varix (Fig. 10). Although embryonic shell growth was not likely simply accretionary like that of post-hatching shell (Landman et al. 1996; De Baets et al. 2015), this pattern may suggest differences in timing of precipitation across the shell. Future analysis will be necessary to disentangle this pattern. The average $\delta^{18}O$ values of embryonic shell across all five ammonites reveals a range of 2.5‰, suggesting that these individuals experienced events in different places or times, likely showing seasonal differences in the timing of spawning like some modern cephalopods (e.g. Worms 1983). The isotope values of embryonic shell of J-215 and J-273 translate to temperatures of 29 and 27ºC ($\delta^{18}O_{SW}$ = -1.0‰), respectively, that could possibly reflect a more nearshore slightly fresh environment or convection of lower $\delta^{18}O$ waters.

The values of $\delta^{18}O$ immediately after hatching (post-varix) in the first postembryonic whorl are the same as those of the varix and lighter than the average of the bivalves. It suggests that the hatchlings did not occupy the same habitat as the ammonite eggs, that is, along the bottom. In summary, compared to the embryonic shell, the varix and post-varix shell may have been secreted in warmer, shallower depths, or possibly fresher near shore environments, but still with salinities ≥ 20‰ based on the salinity tolerances of modern cephalopods (von Boletzky, pers. comm., 2015) although lower salinities (< 20‰) have been suggested from recent paleoclimate modeling (Petersen et al. 2016), but these seem unlikely in light of the present results.

After the first postembryonic whorl in J-215 and J-273 (phragmocone diameters of 5.8 and 2.9 mm, respectively), $\delta^{18}O$ becomes slightly heavier, in the direction of the benthic bivalves. Change in the stable oxygen isotopic composition of ammonites toward bivalves at this

564 growth stage suggests that the ammonites assumed a more demersal, possibly adult-like, habitat
565 after 1 postembryonic whorl (360 degrees growth). In scaphites, minor morphological changes
566 occur at this size, including changes in the size of the umbilicus and the appearance of
567 ornamentation (Landman 1987) that have been interpreted as a shift to a more demersal mode of
568 life. In contrast, in J-125 and J-145, with phragmocone diameters of ≥ 6.5 and 4.8 mm,
569 respectively, $\delta^{18}O$ becomes lower. This may suggest that the individuals remained in shallower
570 water or in more nearshore settings for longer periods of time. In J-209, $\delta^{18}O$ oscillates, and
571 during the end of the second whorl, approaches that of benthic bivalves. This could imply
572 vertical movement in the water column, or transport through variable $\delta^{18}O_{SW}$. It is possible that
573 the presence of short pathological varices is reflected in δ18O patterns like those in J-125 and J-
574 145 (Table 1, Fig. 10); however, J-209 exhibits similar varices but a stepwise change more like
575 that of J-215 and J-273 (Fig. 10).

576 *Carbon Isotopes.—*

577 Variation in mollusk shell $\delta^{13}C$ is caused by changing $\delta^{13}C$ of either diet or DIC or the
578 ratio of respired C to DIC (McConnaughey and Gillikin 2008). There are three hypotheses that
579 can readily explain the $\delta^{13}C$ shift between the embryonic whorls, varix, and post-hatching
580 ammonite shell: 1) the ratio of respired to ambient CO_2 changes with the removal of the egg-
581 membrane barrier, 2) $\delta^{13}C$ of yolk and particulate organic matter are dramatically different, and
582 3) the $\delta^{13}C_{DIC}$ gradient is influenced by freshwater input. Our data alone do not provide enough
583 evidence to clearly determine if one change had a greater impact, but we can offer some
584 constraints based on published data from the WIS, $\delta^{13}C_{DIC}$ gradients in modern oceans and
585 aquarium rearing experiments of *Nautilus*.

586 The largest shift in ammonite $\delta^{13}C$ occurs at hatching, between the embryonic shell and
587 the varix. Three major state changes occur at hatching that could have all contributed to the

588 observed shift: 1) Changing diet from yolk to particulate organic matter, 2) Movement to a
589 higher position in the water column, and 3) Leaving the egg membrane and starting to swim by
590 jetting. The diet of embryonic ammonites was sourced solely from the egg yolk, that may be an
591 invariable $\delta^{13}C_{diet}$ reservoir. After hatching, the ammonite diet was likely suspended particulate
592 organic matter that likely had a different $\delta^{13}C$ value than that of the yolk. An aquarium reared
593 *Nautilus* showed an approximately -4‰ shift in $\delta^{13}C$ at hatching while $\delta^{13}C_{DIC}$ was likely
594 constant (Landman et al. 1994).

595 Hatching and moving to a position shallow in the water column would have changed the
596 $\delta^{13}C_{DIC}$ the ammonites were experiencing. Because of the biological pump, most $\delta^{13}C_{DIC}$ profiles
597 in the modern open ocean or Black Sea show surface water with higher $\delta^{13}C$ values and lower
598 $\delta^{13}C$ values lower in the water column (Kroopnick 1985). This profile may not hold true in the
599 WIS where brackish water is an important control on the vertical structure of the seaway
600 (Petersen et al. 2016). Freshwater $\delta^{13}C_{DIC}$ is strongly influenced by the degradation of terrestrial
601 organic matter and often has low $\delta^{13}C$ values (Amiotte-Suchet et al. 1999). Bivalves (*Unio*)
602 measured from time equivalent Hell Creek Formation have carbon isotope values of ~-4‰
603 (VPDB) which indicates relatively low values can be expected for surface waters, especially
604 during seasons of high freshwater discharge (Cochran et al. 2003).

605 The presence of the egg membrane may have caused more respired CO_2 to be
606 incorporated into the ammonite shell before hatching or could have preferentially trapped more
607 heavy carbon, creating a different $\delta^{13}C_{DIC}$ in the egg than that of ambient seawater. However, the
608 potential magnitude of these effects has not been calibrated with modern experimental studies on
609 macroinvertebrates. An additional membrane separating the mantle fluids (where calcification
610 occurs) from ambient seawater could cause a fractionation because of preferential ^{12}C loss in the
611 form of CO_2 and retention of ^{13}C as HCO_3 (McConnaughey and Gillikin 2008). The magnitude

612 of this fractionation would depend on diffusion rates across the membrane and therefore the
613 difference in pCO_2 between the egg case and the ambient environment. Hatching removes the
614 egg case barrier, exposing the ammonite to ambient $\delta^{13}C_{DIC}$ and changes the difference in pCO_2
615 across the mantle membrane (Melzner et al. 2009). Active ventilation presumably also starts at
616 hatching and may increase the amount of ambient CO_2 incorporated into the shell. To explain the
617 $\delta^{13}C$ signal with a constant value of respired $\delta^{13}C$ and $\delta^{13}C_{DIC}$ would require a shift in the
618 proportion of respired CO_2 incorporated comparable to ontogenetic changes in larger (~10 – 100
619 mm) bivalves (~10 – 40% respired carbon) and is therefore unlikely (Gillikin et al. 2007;
620 McConnaughey and Gillikin 2008).

621 A dietary shift from yolk to particulate organic matter or vertical movement in the water
622 column are possible causes of the pre- to post-hatching shift in $\delta^{13}C$. A change in depth is
623 consistent with the $\delta^{18}O$ shifts observed between embryonic shell and varix values in the shells
624 that indicate transition to warmer or fresher water. A pre-to-post hatching dietary $\delta^{13}C$ must
625 necessarily occur because of the loss of yolk as a carbon source at hatching. Aquarium studies
626 investigating the $\delta^{13}C_{DIC}$ of *Nautilus* or other extant cephalopods could provide constraints on the
627 magnitude of change that hatching itself causes by the removal of an additional membrane.

628 *Comparison with Co-occurring Nautilids.—*

629 The isotope patterns in these five ammonites are distinctly different from a nautilid
630 sampled from a different concretion in the Fox Hills Formation (FH1 in Landman et al., 1983;
631 reproduced here as Fig. 13). In *Eutrephocoeras dekayi* hatching occurs between septa 4 and 5.
632 The values of $\delta^{18}O$ in the pre-hatching septa (3 and 4) average -0.1‰. The average value of the
633 next 16 septa is 0.4‰, suggesting that there is almost no net change between the embryonic and
634 postembryonic habitat compared to the transition in the ammonites (Figs. 8 and 12, Table 2). No
635 major transition is apparent in the $\delta^{13}C$ between septa 4 and 5, however a transition of +0.5‰ is

present between septa 9 and 10. Like modern *Nautilus*, the eggs of *E. dekayi* must have been laid on the bottom, and the newly hatched animal must have also lived close to the bottom.

Concretion Accumulation and Paleoenvironmental Interpretation

Despite their various ontogenetic trajectories, all the studied specimens are preserved in the same concretion. They died at a diameter of 2.9 to 7.8 mm corresponding to a phragmocone diameter of 1.7 to ≥6.5 mm. This corresponds to the size peak of the juveniles in this and associated concretions. The silty lithology and the presence of abundant plant debris suggest that they were deposited in a nearshore environment at the base of the lower shoreface transition zone (Landman and Waage 1993). The presence of comminuted plant fragments, jaws and hook-like structures outside of body chambers, and broken apertures on the juveniles suggest that the scaphites were subjected to some post-mortem transportation and abrasion. The fact that the phragmocones are filled with calcite and the body chambers are filled with sediment, however, suggests that the process did not permit sediment transport into the phragmocones through breakage or infiltration through the siphuncle. Accumulations, such as these, consisting almost exclusively of juveniles in the Fox Hills Formation are only known from this horizon between the Timber Lake and Trail City Members (Figs 2 and 7).

Waage (1965, 1968) inferred the presence of a northeast-southwest trending current that possibly paralleled the coastline in north-central South Dakota during the deposition of the Fox Hills Formation. The current is inferred based on the increase in siltier/sandier sediments up-section toward the southwest, and the general geometry of a coarser sand body (Waage 1965, 1968). The newly hatched ammonites may have been caught up in this current, permitting wide dispersal. The environment, much like other near-coastline environments in the WIS, may have also been influenced by hyperpycnal and hypopycnal flows sourced from nearby rivers (Bhattacharya and MacEachern 2009). Normal and reverse bedding indicative of hyperpycnal

660 flows have not been reported in the Fox Hills Formation of South Dakota, perhaps due to
661 extensive bioturbation (Waage 1968). Such episodic flows, often triggered by storms, would
662 have coincided with plumes of freshwater discharge that were threatening to ammonites and
663 other stenotopic organisms. Transport of sediments from near shore containing plant material
664 would also have occurred.

665 *Western Interior Seaway Paleoceanography.—*

666 Unlike much of the previous work on WIS paleoceanography (Cochran et al. 2003;
667 Dennis et al. 2013; Petersen et al. 2016), our data describe the paleoenvironment on a small
668 spatial (10's to 100's of m) and temporal (months to decades) scale. Modern datasets of $\delta^{18}O_{SW}$
669 for nearshore surface water collected on the decadal scale exhibit high spatial and seasonal
670 variability (3-4‰, with salinities >20‰, (Whitney et al. 2017). The range of $\delta^{18}O$ and $\delta^{13}C$
671 within and between individual ammonites and bivalves indicates that significant spatial and
672 temporal heterogeneity in the salinity or temperature was present in the WIS. The range of $\delta^{18}O$
673 within ammonites is likely to reflect both temperature and salinity effects. Large $\delta^{13}C$ gradients
674 of 5-6‰ may have existed within the water column, with the surface water dominated by fresher
675 water with low $\delta^{13}C_{DIC}$, and then pore fluid being dominated by even lower $\delta^{13}C_{DIC}$ caused by
676 the degradation of organic matter. Large temperature gradients (~20 °C) are also indicated by our
677 data if uniform $\delta^{18}O_{water}$ through the water column is assumed, however, nearshore $\delta^{18}O_{water}$ is
678 suggested to have had a range of -8 to -2‰ (Petersen et al. 2016). Our data suggest extremely
679 low $\delta^{18}O_{SW}$ values were unlikely unless nearer shore than our sampling location. Perhaps this
680 oceanographic heterogeneity drove endemism (Myers et al. 2012) in the WIS and could drive
681 differences in evolutionary kinetics between epeiric seaways and the open ocean (Peters 2007;
682 Miller and Foote 2009).

683 **Conclusions**

Authigenic calcite, bivalve calcite, and ammonite aragonite have distinct $\delta^{13}C$ and $\delta^{18}O$ values in the Fox Hills Formation concretion. Authigenic calcite has more positive $\delta^{18}O$ (~-0.6‰, VPDB) and much more negative $\delta^{13}C$ (~-24‰, VPDB) than either bivalve or ammonite material. There is some range of $\delta^{18}O$ within bivalves, but individuals do not exhibit complete seasonal sinusoids. Embryonic ammonite shell has the highest $\delta^{18}O$ (~-2‰, VPDB) and $\delta^{13}C$ (~+5‰, VPDB) values within the ammonites and the values approach on those of the bivalves. Ammonite shell values change noticeably at the varix (average change embryonic to varix $\delta^{18}O$ +1‰, $\delta^{13}C$ -5‰), when hatching is inferred to have occurred. Two patterns of stepwise change in $\delta^{18}O$ are present in post-hatching ammonite shells. Three shells show a more positive shift of ~1‰ and two show more negative shift of ~1‰. No differences in $\delta^{18}O$ or $\delta^{13}C$ were detectable between the nacreous or prismatic layers of the ammonite shell.

Hoploscaphites comprimus in the Fox Hills Formation appear to have eggs that developed near the sea floor. The similarity in $\delta^{18}O$ and $\delta^{13}C$ between bivalves and embryonic ammonite shell suggests that these individuals developed in the lower water column. Upon hatching, the ammonites all moved into either a warmer or more brackish habitat, both of which were likely characteristic of shallower water environments that were accessible to slow swimming hatchlings. Such a scenario suggests a planktic mode of life for hatchlings and corroborates inferences about a planktic stage based on buoyancy, stratigraphic occurrence, and analogy to the modern cephalopods (e.g. Ritterbush et al. 2014; De Baets et al. 2015). A stepwise transition in $\delta^{18}O$ near one whorl growth in all five ammonites suggests a return to a nektobenthic mode of life for some individuals and/or a movement nearshore for others. Our data also strongly support the occasional, perhaps seasonal, development of strong water column thermohaline stratification in the WIS (e.g. Kump and Slingerland 1999; Petersen et al. 2016). Future SIMS studies of embryonic ammonite shell and environmental context from foraminifera

or benthic mollusks will have the potential to determine the prevalence of complex water column occupation strategies during early ontogeny.

These data show variability in both habitat occupied and seasonal timing of development of several individuals from the same ammonite species that lived at nearly the same time. Similar patterns of seasonally protracted spawning are known from modern organisms, but it is important to appreciate this variability when attempting to understand proximal causes of extinction based on patterns in the fossil record. Scaphites were one of the few short-term survivors at the K-Pg (Landman et al. 2014), and perhaps it was this breadth of developmental timing and environment that promoted both wide geographic distribution and survival.

Acknowledgments

We thank B. Hess for sample preparation; P. Gopon, Z. D. Michels, and J. Fournelle for assistance with SEM analysis; A. C. Denny and J. N. Cammack for development of QGIS workflow; G. L. Wolfe, M. Baddouh, J. Wycech, S. K. McMullen, and D. C. Kelly for discussion of this project. We also wish to thank K. De Baets and two anonymous reviewer for their comments on this manuscript. This work was supported by a Geological Society of America Graduate Student Research Grant, the Norman Newell Fund at the American Museum of Natural History, and the Department of Geoscience at the University of Wisconsin – Madison. WiscSIMS is supported by the National Science Foundation (EAR13-55590) and the University of Wisconsin-Madison.

729 **Literature Cited**

730 Aguiar, D. C. de, C. L. D. B. Rossi-Wongtschowski, and J. A. A. Perez. 2012. Validation of
731 daily growth increments of statoliths of Brazilian squid *Doryteuthis plei* and *D.*
732 *sanpaulensis* (Cephalopoda. Loliginidae). Bioikos 26:13–21.

733 Allison, P. A., and K. Pye. 1994. Early diagenetic mineralization and fossil preservation in
734 modern carbonate concretions. PALAIOS 9:561–575.

735 Amiotte-Suchet, P., D. Aubert, J. L. Probst, F. Gauthier-Lafaye, A. Probst, F. Andreux, and D.
736 Viville. 1999. $\delta^{13}C$ pattern of dissolved inorganic carbon in a small granitic catchment:
737 the Strengbach case study (Vosges Mountains, France). Chemical Geology 159:129–145.

738 Arkhipkin, A. I., and V. V. Laptikhovsky. 2012. Impact of ocean acidification on plankton larvae
739 as a cause of mass extinctions in ammonites and belemnites. Neues Jahrbuch für
740 Geologie und Paläontologie - Abhandlungen 266:39–50.

741 Aubert, M., I. S. Williams, K. Boljkovac, I. Moffat, M.-H. Moncel, E. Dufour, and R. Grün.
742 2012. In situ oxygen isotope micro-analysis of faunal material and human teeth using a
743 SHRIMP II: a new tool for palaeo-ecology and archaeology. Journal of Archaeological
744 Science 39:3184–3194.

745 Bhattacharya, J. P., and J. A. MacEachern. 2009. Hyperpycnal rivers and prodeltaic shelves in
746 the Cretaceous seaway of North America. Journal of Sedimentary Research 79:184–209.

747 Boletzky, S. v. 1983: Embyronic phase. Pp. 5–31 *in* P. R. Boyle, ed. Cephalopod Life Cycles,
748 Vol. II. Comparative Reviews. Academic Press, London.

749 Boletzky, S. von. 1978. Nos connaissances actuelles sur le développement des Octopodes. Vie
750 Milieu 28:85–120.

751 Bucher, H., N. H. Landman, S. M. Klofak, and J. Guex. 1996. Mode and Rate of Growth in
752 Ammonoids. Pp.407–461 *in* N. H. Landman, K. Tanabe, and R. A. Davis, eds.
753 Ammonoid Paleobiology. Plenum, New York.
754 Cherns, L., and V. P. Wright. 2000. Missing molluscs as evidence of large-scale, early skeletal
755 aragonite dissolution in a Silurian sea. Geology 28:791–794.
756 Clements, T., C. Colleary, K. De Baets, and J. Vinther. 2017. Buoyancy mechanisms limit
757 preservation of coleoid cephalopod soft tissues in Mesozoic Lagerstätten. Palaeontology
758 60:1–14.
759 Cobban, W. A., E. A. Merewether, T. D. Fouch, and J. D. Obradovich. 1994. Some Cretaceous
760 Shorelines in the Western Interior of the United States. Pp.393–425 *in* M. V. Caputo, J.
761 A. Peterson, and K. J. Franczyk, eds. Mesozoic Systems of the Rocky Mountain Region,
762 USA. The Rocky Mountain Section SEPM, Denver.
763 Cochran, J. K., N. H. Landman, K. K. Turekian, A. Michard, and D. P. Schrag. 2003.
764 Paleoceanography of the Late Cretaceous (Maastrichtian) Western Interior Seaway of
765 North America: evidence from Sr and O isotopes. Palaeogeography, Palaeoclimatology,
766 Palaeoecology 191:45–64.
767 Cusack, M., J. England, P. Dalbeck, A. W. Tudhope, A. E. Fallick, and N. Allison. 2008.
768 Electron backscatter diffraction (EBSD) as a tool for detection of coral diagenesis. Coral
769 Reefs 27:905–911.
770 De Baets, K., C. Klug, and D. Korn. 2011. Devonian pearls and ammonoid-endoparasite co-
771 evolution. Acta Palaeontologica Polonica 56:159–180.
772 De Baets, K., N. H. Landman, and K. Tanabe. 2015. Ammonoid Embryonic Development.
773 Pp.113–205 *in* C. Klug, D. Korn, K. De Baets, I. Kruta, and R. H. Mapes, eds.
774 Ammonoid Paleobiology: From Anatomy to Ecology. Springer Netherlands.

De Baets, K., C. Klug, D. Korn, and N. H. Landman. 2012. Early Evolutionary Trends in Ammonoid Embryonic Development. Evolution 66:1788–1806.

Dennis, K. J., J. K. Cochran, N. H. Landman, and D. P. Schrag. 2013. The climate of the Late Cretaceous: New insights from the application of the carbonate clumped isotope thermometer to Western Interior Seaway macrofossil. Earth and Planetary Science Letters 362:51–65.

Dutton, A., B. T. Huber, K. C. Lohmann, and W. J. Zinsmeister. 2007. High-resolution stable isotope profiles of a dimitobelid belemnite: implications for paleodepth habitat and Late Maastrichtian climate seasonality. PALAIOS 22:642–650.

Etches, S., J. Clarke, and J. Callomon. 2009. Ammonite eggs and ammonitellae from the Kimmeridge Clay Formation (Upper Jurassic) of Dorset, England. Lethaia 42:204–217.

Fatherree, J. W., P. J. Harries, and T. M. Quinn. 1998. Oxygen and carbon isotopic "dissection" of *Baculites compressus* (Mollusca: Cephalopoda) from the Pierre Shale (upper Campanian) of South Dakota; implications for paleoenvironmental reconstructions. PALAIOS 13:376–385.

Fisher, C. G., and M. A. Arthur. 2002. Water mass characteristics in the Cenomanian US Western Interior seaway as indicated by stable isotopes of calcareous organisms. Palaeogeography, Palaeoclimatology, Palaeoecology 188:189–213.

Forsythe, J. W., and W. J. Van Heukelem. 1987. Growth. Pp.135–156 *in* P. R. Boyle, ed. Cephalopod Life Cycles, Vol. II. Comparative Reviews. Academic Press, London.

Gill, J. R., and W. A. Cobban. 1966. The Red Bird section of the Upper Cretaceous Pierre Shale in Wyoming, with a section on a new echinoid from the Cretaceous Pierre Shale of eastern Wyoming. U.S. Geological Survey Professional Paper. 393-A:1-73.

798 Gillikin, D. P., A. Lorrain, L. Meng, and F. Dehairs. 2007. A large metabolic carbon contribution
799 to the $\delta^{13}C$ record in marine aragonitic bivalve shells. Geochimica et Cosmochimica Acta
800 71:2936–2946.
801 Grossman, E. L., and T.-L. Ku. 1986. Oxygen and carbon isotope fractionation in biogenic
802 aragonite: Temperature effects. Chemical Geology: Isotope Geoscience section 59:59–74.
803 Hain, M. P., D. M. Sigman, and G. H. Haug. 2014. 8.18 - The Biological Pump in the Past.
804 Pp.485–517 *in* H. D. Holland and K. K. Turekian, eds. Treatise on Geochemistry (Second
805 Edition). Elsevier, Oxford.
806 Hein, J. R., W. R. Normark, B. R. McIntyre, T. D. Lorenson, and C. L. Powell. 2006.
807 Methanogenic calcite, ^{13}C-depleted bivalve shells, and gas hydrate from a mud volcano
808 offshore southern California. Geology 34:109–112.
809 Ivany, L. C. 2012. Reconstructing paleoseasonality from accretionary skeletal carbonates -
810 Challenges and opportunities. *In* L. C. Ivany and B. T. Huber, eds. Earth's deep-time
811 climate - the state of the art in 2012, Paleontological Society Short Course, November 3,
812 2012. Paleontological Society Papers 18:133-165.
813 Ivany, L. C., B. H. Wilkinson, and D. S. Jones. 2003. Using Stable Isotopic Data to Resolve Rate
814 and Duration of Growth throughout Ontogeny: An Example from the Surf Clam, *Spisula*
815 *solidissima*. PALAIOS 18:126–137.
816 Jablonski, D., and G. Hunt. 2006. Larval ecology, geographic range, and species survivorship in
817 Cretaceous mollusks: organismic versus species-level explanations. The American
818 Naturalist 168:556–564.
819 Jacobs, D. K., and N. H. Landman. 1993. *Nautilus*—a poor model for the function and behavior
820 of ammonoids? Lethaia 26:101–111.

821 Jacobs, D. K., and J. A. Chamberlain. 1996. Buoyancy and Hydrodynamics in Ammonoids.
822 Pp.169–224 *in* N. H. Landman, K. Tanabe, and R. A. Davis, eds. Ammonoid
823 Paleobiology. Plenum, New York.
824 Jacobs, D. K., N. H. Landman, and J. A. Chamberlain. 1994. Ammonite shell shape covaries
825 with facies and hydrodynamics: iterative evolution as a response to changes in basinal
826 environment. Geology 22:905–908.
827 Jones, D. S. 1983. Sclerochronology: reading the record of the molluscan shell. American
828 Scientist 71:384–391.
829 Killick, R., and I. Eckley. 2014. changepoint: An R package for changepoint analysis. Journal of
830 Statistical Software 58:1–19.
831 Killingley, J. S., and W. H. Berger. 1979. Stable isotopes in a mollusk shell: detection of
832 upwelling events. Science 205:186–188.
833 Kim, S.-T., A. Mucci, and B. E. Taylor. 2007a. Phosphoric acid fractionation factors for calcite
834 and aragonite between 25 and 75 °C: revisited. Chemical Geology 246:135–146.
835 Kim, S.-T., J. R. O'Neil, C. Hillaire-Marcel, and A. Mucci. 2007b. Oxygen isotope fractionation
836 between synthetic aragonite and water: influence of temperature and Mg2+
837 concentration. Geochimica et Cosmochimica Acta 71:4704–4715.
838 Kita, N. T., T. Ushikubo, B. Fu, and J. W. Valley. 2009. High precision SIMS oxygen isotope
839 analysis and the effect of sample topography. Chemical Geology 264:43–57.
840 Klug, C., W. Riegraf, and J. Lehmann. 2012. Soft–part preservation in heteromorph ammonites
841 from the Cenomanian–Turonian Boundary Event (OAE 2) in north–west Germany.
842 Palaeontology 55:1307–1331.
843 Knoll, A. H., R. K. Bambach, J. L. Payne, S. Pruss, and W. W. Fischer. 2007. Paleophysiology
844 and end-Permian mass extinction. Earth and Planetary Science Letters 256:295–313.

845 Kozdon, R., T. Ushikubo, N. T. Kita, M. Spicuzza, and J. W. Valley. 2009. Intratest oxygen
846 isotope variability in the planktonic foraminifer *N. pachyderma*: real vs. apparent vital
847 effects by ion microprobe. Chemical Geology 258:327–337.
848 Kozdon, R., D. C. Kelly, K. Kitajima, A. Strickland, J. H. Fournelle, and J. W. Valley. 2013. In
849 situ $\delta^{18}O$ and Mg/Ca analyses of diagenetic and planktic foraminiferal calcite preserved
850 in a deep-sea record of the Paleocene-Eocene thermal maximum. Paleoceanography
851 28:517–528.
852 Kröger, B., J. Vinther, and D. Fuchs. 2011. Cephalopod origin and evolution: A congruent
853 picture emerging from fossils, development and molecules. BioEssays 33:602–613.
854 Kroopnick, P., R. F. Weiss, and H. Craig. 1972. Total CO_2,^{13}C, and dissolved oxygen ^{18}O at
855 Geosecs II in the North Atlantic. Earth and Planetary Science Letters 16:103–110.
856 Kroopnick, P. M. 1985. The distribution of ^{13}C of ΣCO_2 in the world oceans. Deep Sea Research
857 Part A. Oceanographic Research Papers 32:57–84.
858 Kruta, I., N. H. Landman, and J. K. Cochran. 2014. A new approach for the determination of
859 ammonite and nautilid habitats. PLoS ONE 9:e87479.
860 Kulicki, C. 1996. Ammonoid Shell Microstructure. Pp.65–101 *in* N. H. Landman, K. Tanabe,
861 and R. A. Davis, eds. Ammonoid Paleobiology. Plenum Press, New York.
862 Kump, L. R., and R. L. Slingerland. 1999. Circulation and stratification of the early Turonian
863 Western Interior Seaway: Sensitivity to a variety of forcings. Pp.181–190 *in* E. Barrera
864 and C. C. Johnson, eds. Evolution of the Cretaceous Ocean–Climate System. Geological
865 Society of America Special Paper 332.
866 Landman, N. H. 1987. Ontogeny of Upper Cretaceous (Turonian-Santonian) scaphitid
867 ammonites from the Western Interior of North America: Systematics, developmental

patterns, and life history. Bulletin of the American Museum of Natural History 185:117–241.

Landman, N. H., and J. K. Cochran. 2010. Growth and longevity of *Nautilus*. Pp.401–420 *in* W. B. Saunders and N. H. Landman, eds. *Nautilus*: The Biology and Paleobiology of a Living Fossil. Topics in Geobiology Vol. 6. Springer, Dordrecht.

Landman, N. H., and K. M. Waage. 1993. Scaphitid ammonites of the Upper Cretaceous (Maastrichtian) Fox Hills Formation in South Dakota and Wyoming. Bulletin of the American Museum of Natural History 215:1–257.

Landman, N. H., and W. A. Cobban. 2007. Redescription of the Late Cretaceous (Late Santonian) ammonite *Desmoscaphites bassleri* Reeside, 1927, from the Western Interior of North America. Rocky Mountain Geology 42:67–94.

Landman, N. H., and S. M. Klofak. 2012. Anatomy of a concretion: life, death and burial in the Western Interior Seaway. PALAIOS 27:672–693.

Landman, N. H., D. M. Rye, and K. L. Shelton. 1983. Early ontogeny of *Eutrephoceras* compared to recent *Nautilus* and Mesozoic ammonites: evidence from shell morphology and light stable isotopes. Paleobiology 9:269–279.

Landman, N. H., K. Tanabe, and Y. Shigeta. 1996. Ammonoid Embryonic Development. Pp.343–405 *in* N. H. Landman, K. Tanabe, and R. A. Davis, eds. Ammonoid Paleobiology. Plenum Press, New York.

Landman, N. H., S. M. Klofak, and K. B. Sarg. 2008. Variation in Adult Size of Scaphitid Ammonites from the Upper Cretaceous Pierre Shale and Fox Hills Formation. Pp.149–194 *in* High-Resolution Approaches in Stratigraphic Paleontology. Springer, Dordrecht.

Landman, N. H., W. A. Cobban, and N. L. Larson. 2012a. Mode of life and habitat of scaphitid ammonites. Geobios 45:87–98.

892 Landman, N. H., Z. Remin, M. P. Garb, and J. A. Chamberlain Jr. 2013. Cephalopods from the
893 Badlands National Park area, South Dakota: Reassessment of the position of the
894 Cretaceous/Paleogene boundary. Cretaceous Research 42:1–27.
895 Landman, N. H., J. K. Cochran, D. M. Rye, K. Tanabe, and J. M. Arnold. 1994. Early life history
896 of *Nautilus*: evidence from isotopic analyses of aquarium-reared specimens. Paleobiology
897 20:40–51.
898 Landman, N. H., J. C. Grier, J. W. Grier, J. K. Cochran, and S. M. Klofak. 2015: 3-D orientation
899 and distribution of ammonites in a concretion from the Upper Cretaceous Pierre Shale of
900 Montana. Swiss Journal of Palaeontology 134:257–279.
901 Landman, N. H., J. K. Cochran, N. L. Larson, J. Brezina, M. P. Garb, and P. J. Harries. 2012b.
902 Methane seeps as ammonite habitats in the U.S. Western Interior Seaway revealed by
903 isotopic analyses of well-preserved shell material. Geology 40:507–510.
904 Landman, N. H., S. Goolaerts, J. W. M. Jagt, E. A. Jagt-Yazykova, M. Machalski, and M. M.
905 Yacobucci. 2014. Ammonite extinction and nautilid survival at the end of the Cretaceous.
906 Geology 42:707–710.
907 Lécuyer, C., and H. Bucher. 2006. Stable isotope compositions of a late Jurassic ammonite shell:
908 a record of seasonal surface water temperatures in the southern hemisphere? eEarth
909 Discussions 1:1–19.
910 Lemanis, R., S. Zachow, F. Fusseis, and R. Hoffmann. 2015. A new approach using high-
911 resolution computed tomography to test the buoyant properties of chambered cephalopod
912 shells. Paleobiology 41:313–329.
913 Linzmeier, B. J., R. Kozdon, S. E. Peters, and J. W. Valley. 2016. Oxygen Isotope Variability
914 within *Nautilus* Shell Growth Bands. PLOS ONE 11:e0153890.

915 Linzmeier, B. J., K. Kitajima, A. C. Denny, and J. N. Cammack. 2018. QGIS as a tool for the
916 integration of extensive *in situ* microanalytical datasets. Eos, Transactions American
917 Geophysical Union, Accepted.
918 Lukeneder, A. 2015. Ammonoid habitats and life History. Pp.689–791 *in* C. Klug, D. Korn, K.
919 D. Baets, I. Kruta, and R. H. Mapes, eds. Ammonoid Paleobiology: From Anatomy to
920 Ecology. Springer Netherlands.
921 Lukeneder, A., M. Harzhauser, S. Müllegger, and W. E. Piller. 2010. Ontogeny and habitat
922 change in Mesozoic cephalopods revealed by stable isotopes ($\delta^{18}O$, $\delta^{13}C$). Earth and
923 Planetary Science Letters 296:103–114.
924 Macintyre, I. G., and R. P. Reid. 1995. Crystal alteration in a living calcareous alga (*Halimeda*):
925 Implications for studies in skeletal diagenesis. Journal of Sedimentary Research 65:143–
926 153.
927 Mapes, R. H., and A. Nützel. 2009. Late Palaeozoic mollusc reproduction: cephalopod egg-
928 laying behavior and gastropod larval palaeobiology. Lethaia 42:341–356.
929 McConnaughey, T. A., and D. P. Gillikin. 2008. Carbon isotopes in mollusk shell carbonates.
930 Geo-Marine Letters 28:287–299.
931 McCorkle, D. C., S. R. Emerson, and P. D. Quay. 1985. Stable carbon isotopes in marine
932 porewaters. Earth and Planetary Science Letters 74:13–26.
933 McCorkle, D. C., B. H. Corliss, and C. A. Farnham. 1997. Vertical distributions and stable
934 isotopic compositions of live (stained) benthic foraminifera from the North Carolina and
935 California continental margins. Deep Sea Research Part I: Oceanographic Research
936 Papers 44:983–1024.
937 Melzner, F., M. A. Gutowska, M. Langenbuch, S. Dupont, M. Lucassen, M. C. Thorndyke, M.
938 Bleich, and H. O. Pörtner. 2009. Physiological basis for high CO_2 tolerance in marine

939 ectothermic animals: pre-adaptation through lifestyle and ontogeny? Biogeosciences
940 6:2313–2331.
941 Miller, A. I., and M. Foote. 2009. Epicontinental seas versus open-ocean settings: The kinetics of
942 mass extinction and origination. Science 326:1106–1109.
943 Miller, R. G. 1981. Simultaneous Statistical Inference. *Springer Series in Statistics*. Springer.
944 Mironenko, A. A., and M. A. Rogov. 2015. First direct evidence of ammonoid ovoviviparity.
945 Lethaia 49:245–260.
946 Moriya, K. 2015. Isotope signature of ammonoid shells. Pp.793–836 *in* C. Klug, D. Korn, K. D.
947 Baets, I. Kruta, and R. H. Mapes, eds. Ammonoid Paleobiology: From Anatomy to
948 Ecology. Springer Netherlands.
949 Moriya, K., H. Nishi, H. Kawahata, K. Tanabe, and Y. Takayanagi. 2003. Demersal habitat of
950 Late Cretaceous ammonoids: Evidence from oxygen isotopes for the Campanian (Late
951 Cretaceous) northwestern Pacific thermal structure. Geology 31:167–170.
952 Myers, C. E., R. A. MacKenzie, and B. S. Lieberman. 2012. Greenhouse biogeography: the
953 relationship of geographic range to invasion and extinction in the Cretaceous Western
954 Interior Seaway. Paleobiology 39:135–148.
955 Orland, I. J. 2012. Seasonality from speleothems: High-resolution ion microprobe studies at
956 Soreq Cave, Israel. PhD Dissertation, University of Wisconsin - Madison, 304pp.
957 Orland, I. J., M. Bar-Matthews, N. T. Kita, A. Ayalon, A. Matthews, and J. W. Valley. 2009.
958 Climate deterioration in the Eastern Mediterranean as revealed by ion microprobe
959 analysis of a speleothem that grew from 2.2 to 0.9 ka in Soreq Cave, Israel. Quaternary
960 Research 71:27–35.

961 Orland, I. J., R. L. Edwards, H. Cheng, R. Kozdon, M. Cross, and J. W. Valley. 2015a. Direct
962 measurements of deglacial monsoon strength in a Chinese stalagmite. Geology 43:555–
963 558.
964 Orland, I. J., R. Kozdon, B. J. Linzmeier, J. Wycech, M. G. Śliwiński, K. Kitajima, N. T. Kita,
965 and J. W. Valley. 2015b. Enhancing the Accuracy of Carbonate $\delta^{18}O$ and $\delta^{13}C$
966 Measurements by SIMS. AGU Fall Meeting, Dec. 14-18, San Francisco. Abstr. #:
967 PP52B-03.
968 Payne, J. L., and S. Finnegan. 2007. The effect of geographic range on extinction risk during
969 background and mass extinction. Proceedings of the National Academy of Sciences
970 104:10506–10511.
971 Peters, S. E. 2007. The problem with the Paleozoic. Paleobiology 33:165–181.
972 Peters, S. E., J. M. Husson, and J. Czaplewski. 2018. Macrostrat: a platform for geological data
973 integration and deep-time Earth crust research. EarthArXiv. January 27.
974 doi:10.17605/OSF.IO/YNAXW
975 Petersen, S. V., C. R. Tabor, K. C. Lohmann, C. J. Poulsen, K. W. Meyer, S. J. Carpenter, J. M.
976 Erickson, K. K. S. Matsunaga, S. Y. Smith, and N. D. Sheldon. 2016. Temperature and
977 salinity of the Late Cretaceous Western Interior Seaway. Geology 44:903-906.
978 R Core Team. 2017. R: A language and environment for statistical computing. R Foundation for
979 Statistical Computing, Vienna, Austria. https://www.R-project.org
980 Ritterbush, K. A., R. Hoffmann, A. Lukeneder, and K. De Baets. 2014. Pelagic palaeoecology:
981 The importance of recent constraints on ammonoid palaeobiology and life history.
982 Journal of Zoology 292:229–241.

983 Rocha, F., and Á. Guerra. 1996. Signs of an extended and intermittent terminal spawning in the
984 squids *Loligo vulgaris* Lamarck and *Loligo forbesi* Steenstrup (Cephalopoda:
985 Loliginidae). Journal of Experimental Marine Biology and Ecology 207:177–189.
986 Rocha, F., Á. Guerra, and Á. F. González. 2001. A review of reproductive strategies in
987 cephalopods. Biological Reviews 76:291–304.
988 Rollion-Bard, C., D. Mangin, and M. Champenois. 2007. Development and Application of
989 Oxygen and Carbon Isotopic Measurements of Biogenic Carbonates by Ion Microprobe.
990 Geostandards and Geoanalytical Research 31:39–50.
991 Romanek, C. S., E. L. Grossman, and J. W. Morse. 1992. Carbon isotopic fractionation in
992 synthetic aragonite and calcite: Effects of temperature and precipitation rate. Geochimica
993 et Cosmochimica Acta 56:419–430.
994 Rude, P. D., and R. C. Aller. 1991. Fluorine mobility during early diagenesis of carbonate
995 sediment: An indicator of mineral transformations. Geochimica et Cosmochimica Acta
996 55:2491–2509.
997 Sessa, J. A., M. E. Patzkowsky, and T. J. Bralower. 2009. The impact of lithification on the
998 diversity, size distribution, and recovery dynamics of marine invertebrate assemblages.
999 Geology 37:115–118.
1000 Sessa, J. A., L. C. Ivany, T. H. Schlossnagle, S. D. Samson, and S. A. Schellenberg. 2012. The
1001 fidelity of oxygen and strontium isotope values from shallow shelf settings: Implications
1002 for temperature and age reconstructions. Palaeogeography, Palaeoclimatology,
1003 Palaeoecology 342–343:27–39.
1004 Sessa, J. A., E. Larina, K. Knoll, M. Garb, J. K. Cochran, B. T. Huber, K. G. MacLeod, and N.
1005 H. Landman. 2015. Ammonite habitat revealed via isotopic composition and comparisons

1006 with co-occurring benthic and planktonic organisms. Proceedings of the National
1007 Academy of Sciences 112:15562–15567.
1008 Shackleton, N. J., and J. P. Kennett. 1975. Paleotemperature history of the Cenozoic and the
1009 initiation of Antarctic glaciation: Oxygen and carbon isotope analyses in DSDP Sites
1010 277, 279, and 281. Initial reports of the Deep Sea Drilling Project. 29:743–755.
1011 Shigeta, Y. 1993. Post-hatching early life history of Cretaceous ammonoidea. Lethaia 26:133–
1012 145.
1013 Śliwiński, M. G., K. Kitajima, R. Kozdon, M. J. Spicuzza, J. H. Fournelle, A. Denny, and J. W.
1014 Valley. 2016a. Secondary Ion Mass Spectrometry Bias on Isotope Ratios in Dolomite–
1015 Ankerite, Part I: $\delta^{18}O$ Matrix Effects. Geostandards and Geoanalytical Research 40:157–
1016 172.
1017 ——— 2016b. Secondary Ion Mass Spectrometry Bias on Isotope Ratios in Dolomite–Ankerite,
1018 Part II: $\delta^{13}C$ Matrix Effects. Geostandards and Geoanalytical Research 40:173–184.
1019 Speden, I. G. 1970. The Type Fox Hills Formation, Cretaceous (Maestrichtian), South Dakota
1020 Part 2. Systematics of the Bivalvia. *in Peabody Museum of Natural History Bulletin*. Yale
1021 University, p 222.
1022 Stephen, D. A., K. G. Bylund, P. Garcia, R. D. McShinsky, and H. J. Carter. 2012. Taphonomy
1023 of dense concentrations of juvenile ammonoids in the Upper Cretaceous Mancos Shale,
1024 east-central Utah, USA. Geobios 45:121–128.
1025 Stevens, K., J. Mutterlose, and K. Wiedenroth. 2015. Stable isotope data ($\delta^{18}O$, $\delta^{13}C$) of the
1026 ammonite genus *Simbirskites* — implications for habitat reconstructions of extinct
1027 cephalopods. Palaeogeography, Palaeoclimatology, Palaeoecology 417:164–175.

1028 Stinnesbeck, W., E. Frey, and P. Zell. 2016. Evidence for semi-sessile early juvenile life history
1029 in Cretaceous ammonites. Palaeogeography, Palaeoclimatology, Palaeoecology 457:186–
1030 194.
1031 Summers, W. C. 1983. *Loligo pealei*. Pp.115–142 *in* P. R. Boyle, ed. Cephalopod Life Cycles,
1032 Vol. I. Species Accounts. Academic Press, London.
1033 Tanabe, K., N. H. Landman, and I. Kruta. 2012. Microstructure and mineralogy of the outer
1034 calcareous layer in the lower jaws of Cretaceous Tetragonitoidea and Desmoceratoidea
1035 (Ammonoidea). Lethaia 45:191–199.
1036 Tobin, T. S., A. J. Schauer, and E. Lewarch. 2011. Alteration of micromilled carbonate $\delta^{18}O$
1037 during Kiel Device analysis. Rapid Communications in Mass Spectrometry 25:2149–
1038 2152.
1039 Tomašových, A., J. Schlögl, A. Biroň, N. Hudáčková, and T. Mikuš. 2017. Taphonomic Clock
1040 and Bathymetric Dependence of Cephalopod Preservation in Bathyal, Sediment-Starved
1041 Environments. PALAIOS 32:135–152.
1042 Tsujita, C. J., and G. E.G. Westermann. 1998. Ammonoid habitats and habits in the Western
1043 Interior Seaway: a case study from the Upper Cretaceous Bearpaw Formation of southern
1044 Alberta, Canada. Palaeogeography, Palaeoclimatology, Palaeoecology 144:135–160.
1045 Urey, H. C., H. A. Lowenstam, S. Epstein, and C. R. McKinney. 1951. Measurement of
1046 paleotemperatures and temperatures of England, Denmark, and the Southeastern United
1047 States. GSA Bulletin 62:399–416.
1048 Valley, J. W., and N. T. Kita. 2009. In situ oxygen isotope geochemistry by ion microprobe.
1049 Pp.19–63 *in* M. Fayek, ed. MAC Short Course: Secondary Ion Mass Spectrometry in the
1050 Earth Sciences. Vol. 41.

1051 Vetter, L., R. Kozdon, J. W. Valley, C. I. Mora, and H. J. Spero. 2014. SIMS measurements of
1052 intrashell $\delta^{13}C$ in the cultured planktic foraminifer *Orbulina universa*. Geochimica et
1053 Cosmochimica Acta 139:527–539.
1054 Waage, K. M. 1965. The Late Cretaceous coleoid cephalopod *Actinosepia canadensis*
1055 Whiteaves. *in Postilla*. Vol. 94. Peabody Museum Natural History Yale University, p.
1056 Waage, K. M. 1968. The Type Fox Hills Formation, Cretaceous (Maestrichtian), South Dakota
1057 Part 1. Stratigraphy and Paleoenvironments. *in Peabody Museum of Natural History*
1058 *Bulletin*. Yale University, p 33.
1059 Walter, L. M., S. A. Bischof, W. P. Patterson, T. W. Lyons, R. K. O'Nions, M. Gruszczynski, B.
1060 W. Sellwood, and M. L. Coleman. 1993. Dissolution and Recrystallization in Modern
1061 Shelf Carbonates: Evidence from Pore Water and Solid Phase Chemistry [and
1062 Discussion]. Philosophical Transactions of the Royal Society of London A:
1063 Mathematical, Physical and Engineering Sciences 344:27–36.
1064 Wani, R. 2007. How to recognize in situ fossil cephalopods: evidence from experiments with
1065 modern *Nautilus*. Lethaia 40:305–311.
1066 ——— 2011. Sympatric speciation drove the macroevolution of fossil cephalopods. Geology
1067 39:1079–1082.
1068 Ward, P. D., and K. Bandel. 1987. Life history strategies in fossil cephalopods. Pp.329–350 *in* P.
1069 R. Boyle, ed. Cephalopod Life Cycles, Vol. II. Comparative Reviews. Academic Press,
1070 London.
1071 Westermann, G. E. G. 1996. Ammonid life and habitat. Pp.607–707 *in* N. H. Landman, K.
1072 Tanabe, and R. A. Davis, eds. Ammonid Paleobiology. Vol. 13. Plenum Press, New
1073 York.

1074 Whitney, N. M., A. D. Wanamaker, K. J. Kreutz, and D. S. Introne. 2017. Spatial and temporal
1075 variability in the $\delta^{18}O_w$ and salinity compositions of Gulf of Maine coastal surface waters.
1076 Continental Shelf Research 137:163–171.
1077 Wierzbowski, H. 2007. Effects of pre-treatments and organic matter on oxygen and carbon
1078 isotope analyses of skeletal and inorganic calcium carbonate. International Journal of
1079 Mass Spectrometry 268:16–29.
1080 Worms, J. 1983. *Loligo vulgaris*. Pp.143–157 *in* P. R. Boyle, ed. Cephalopod Life Cycles, Vol. I.
1081 Species Accounts. Academic Press, London.
1082 Wycech, J., D. C. Kelly, R. Kozdon, I. J. Orland, H. J. Spero, and J. W. Valley. 2018.
1083 Comparison of $\delta^{18}O$ analyses on individual planktic foraminifer (*Orbulina universa*)
1084 shells by SIMS and Gas-Source Mass Spectrometry. Chemical Geology 483:119–130.
1085 Zakharov, Y., Y. Shigeta, O. Smyshlyaeva, A. Popov, and A. Ignatiev. 2006. Relationship
1086 between $\delta^{13}C$ and $\delta^{18}O$ values of the Recent *Nautilus* and brachiopod shells in the wild
1087 and the problem of reconstruction of fossil cephalopod habitat. Geosciences Journal
1088 10:331–345.
1089 Zakharov, Y. D., Y. Shigeta, A. M. Popov, T. A. Velivetskaya, and T. B. Afanasyeva. 2011.
1090 Cretaceous climatic oscillations in the Bering area (Alaska and Koryak Upland): Isotopic
1091 and palaeontological evidence. Sedimentary Geology 235:122–131.
1092 Zumholz, K., T. H. Hansteen, A. Klügel, and U. Piatkowski. 2006. Food effects on statolith
1093 composition of the common cuttlefish (*Sepia officinalis*). Marine Biology 150:237–244.
1094
1095

Figure Captions

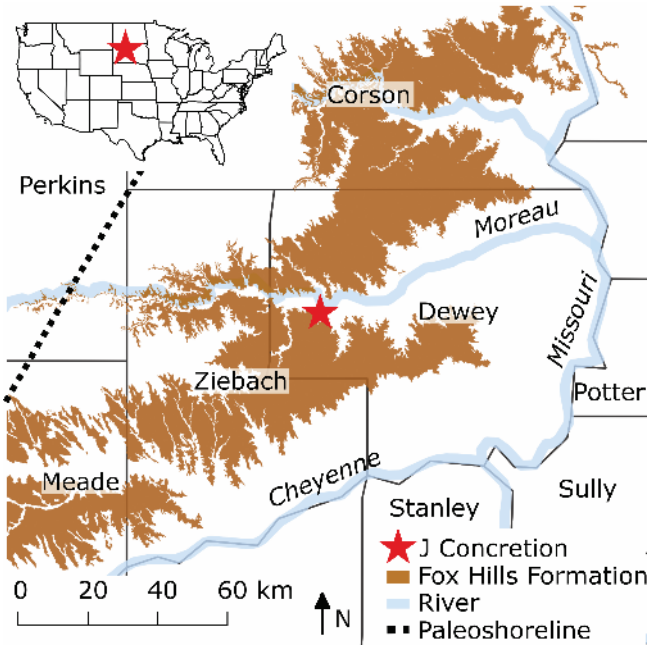

Figure 1. Map showing the location of the J Concretion (red star) and outcrop of the Fox Hills Formation (brown) in north-central South Dakota superimposed over county boundaries. *Hoploscaphites comprimus* are distributed throughout the map area. The map of the Fox Hills Formation is from the Macrostratigraphy Database (Peters et al. 2018). The paleoshoreline is from Landman et al. (2013).

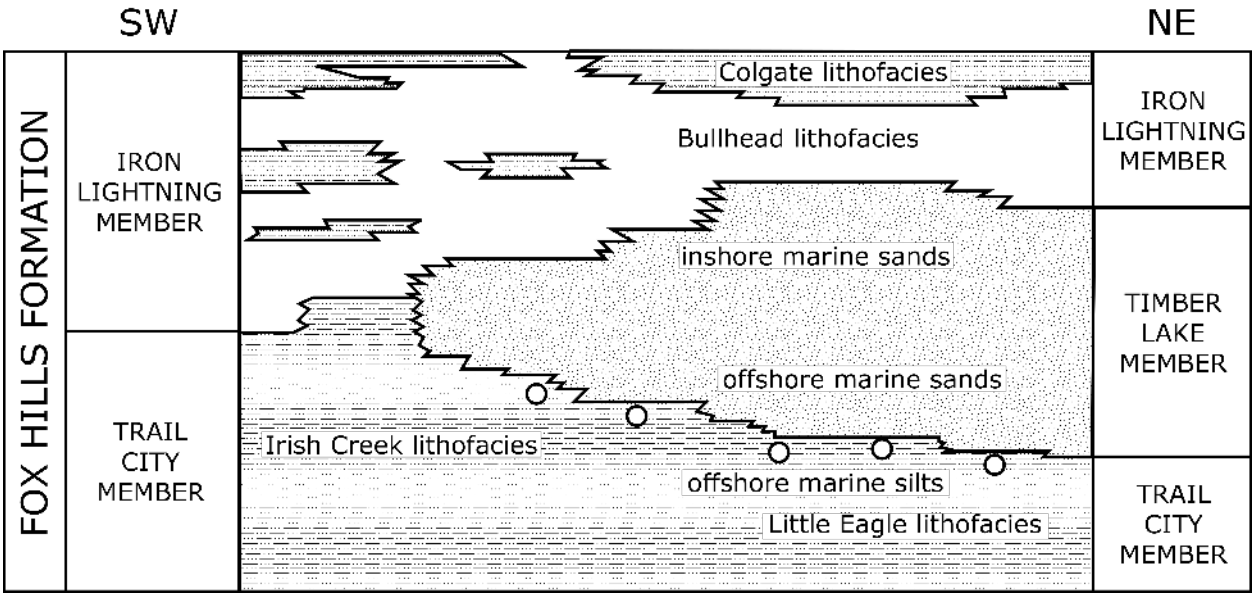

Figure 2. Stratigraphic overview of the Fox Hills Formation indicating the position of the transition concretions (circles), Dewey County, South Dakota. Modified from (Landman and Waage 1993). The concretions occur near the boundary between offshore silts and sands during regression and are likely time-transgressive.

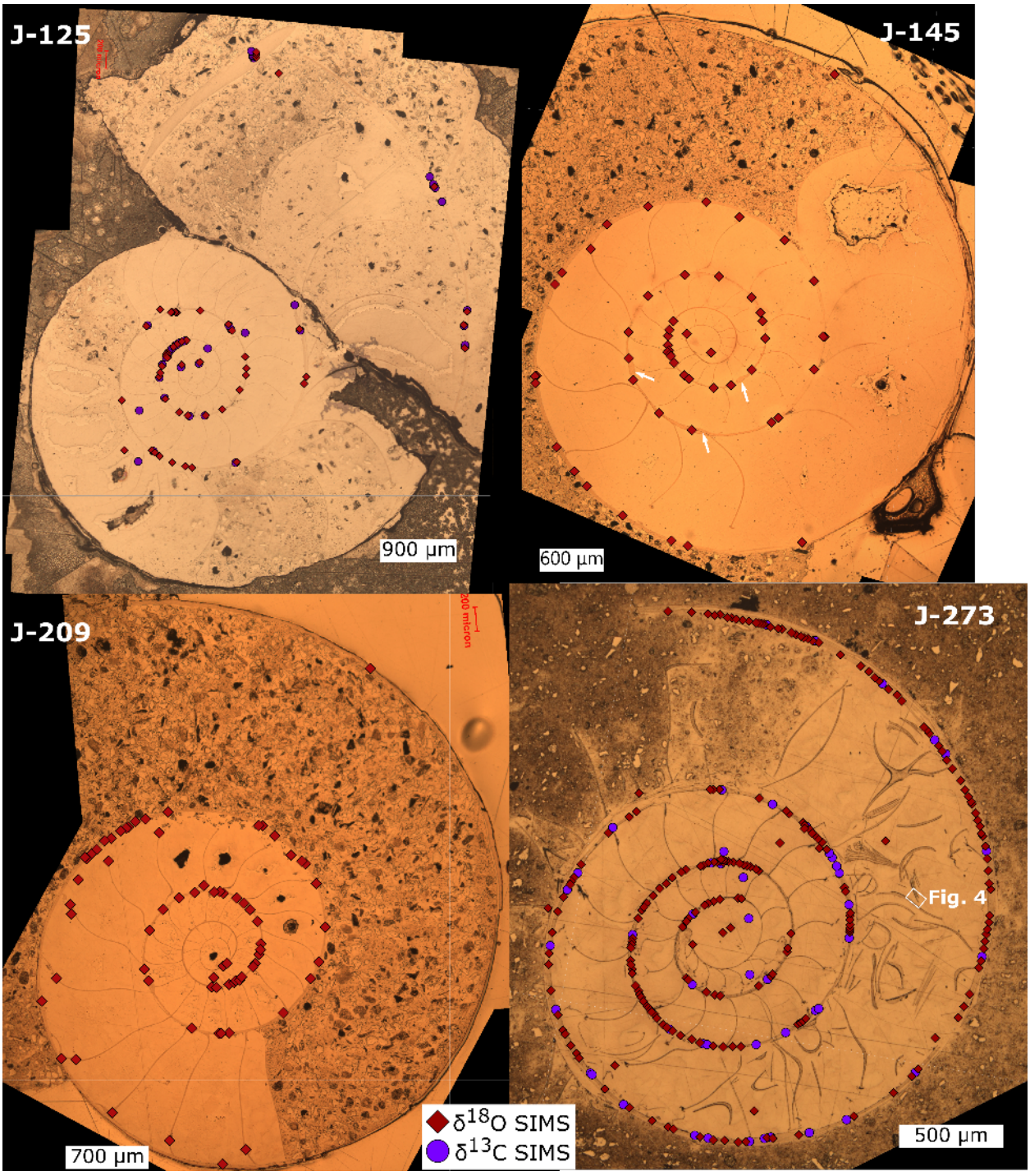

Figure 3. Distribution of $\delta^{18}O$ and $\delta^{13}C$ SIMS pits on cross-sections of *Hoploscaphites comprimus*. Reflected light image of gold-coated samples with the position, but not size, of $\delta^{18}O$ pits indicated by diamonds and $\delta^{13}C$ by circles. Three anomalous post-hatching varixes are highlighted with white arrows on the image of J-145. Early diagenetic calcite fills the chambers at the center of each image. Sediment infills later chambers and surrounds the shells. Septa in

later whorls of J-273 are broken and sometimes wedged apart by the diagenetic calcite (white outlined area, Fig. 4).

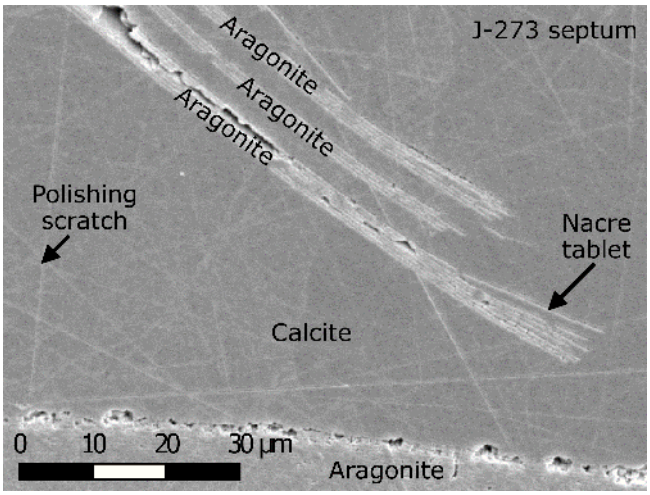

Figure 4. Calcite wedging apart and surrounding nacreous aragonite. The pictured broken septum is from a later whorl of J-273 and is surrounded by diagenetic calcite. Individual layers of nacreous aragonite are split from one another and surrounded by calcite.

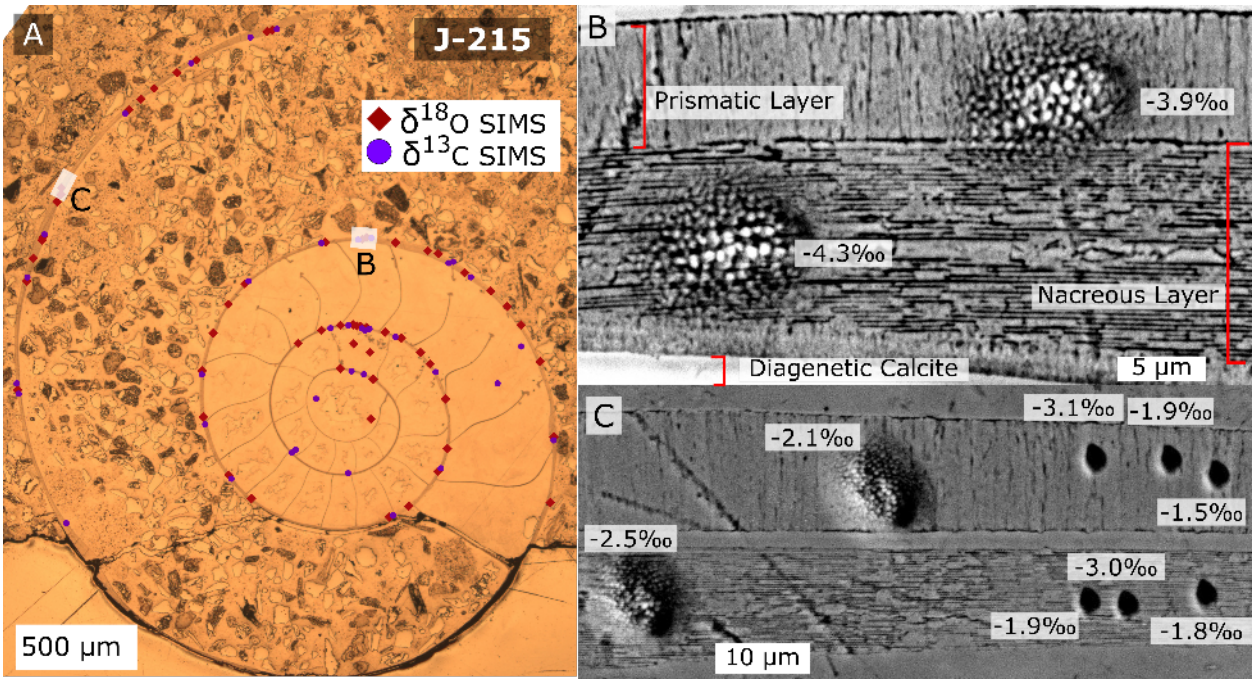

Figure 5. Distribution of $\delta^{18}O$ SIMS pits on a cross-section of *Hoploscaphites comprimus* (J-215) and SEM images of analyzed pits and shell microstructure. A, Reflected light image of gold-coated sample with the position, but not size, of $\delta^{18}O$ (diamonds) and $\delta^{13}C$ (circles) pits on the ammonite shell. B, SEM image of two ~10 µm SIMS pits in the outer prismatic layer and nacreous layer of the shell. The $\delta^{18}O$ values are similar between the two domains given instrumental precision of ±0.3‰ for large pit analyses. C, A comparison of $\delta^{18}O$ measured in the outer prismatic layer and inner nacreous layer with small pit analyses (~3 µm) and large pit (~10 µm) analyses. The $\delta^{18}O$ values of these microstructures are indistinguishable given instrumental precision (3 µm ±0.7‰; 10 µm ±0.3‰).

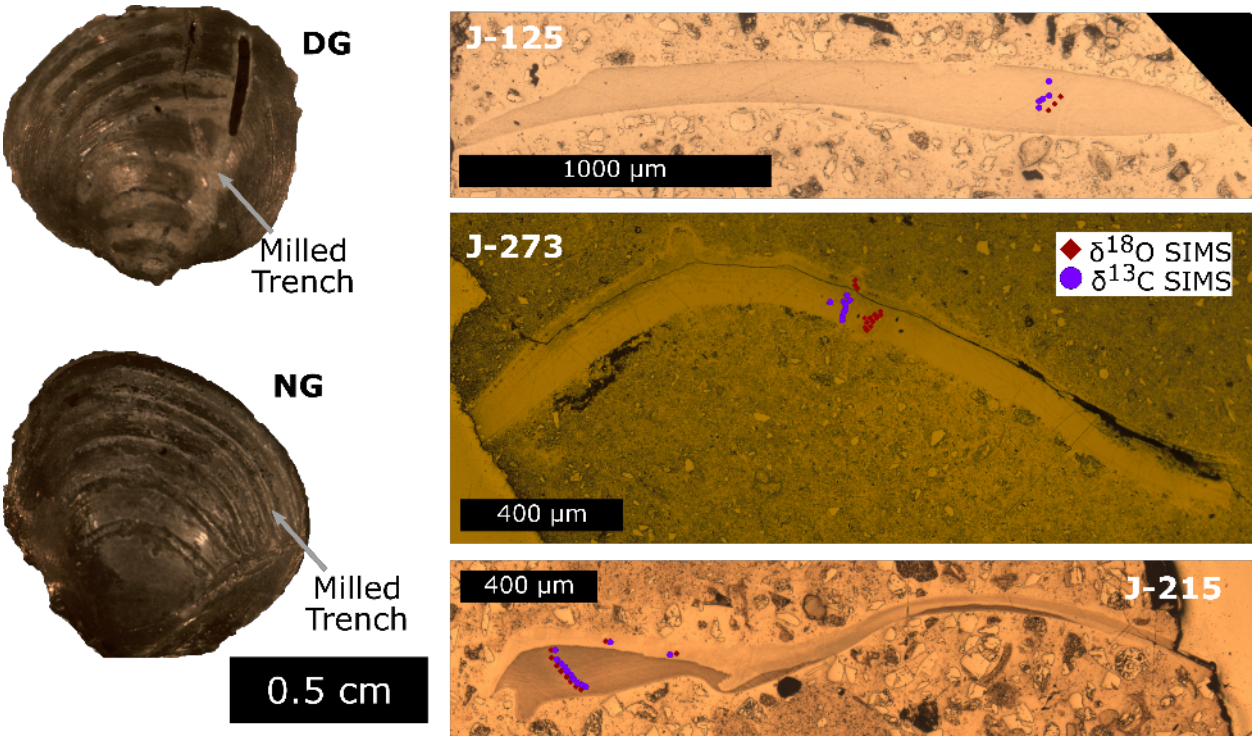

Figure 6. Images of bivalves sampled by milling (DG and NG) and samples measured by SIMS (J-125, J-273, and J-215). Trenches from hand-held drill are visible in the images of NG and DG bivalves. NG and DG are Protocardia. SIMS analysis pits are highlighted by circles ($\delta^{13}C$) and diamonds ($\delta^{18}O$).

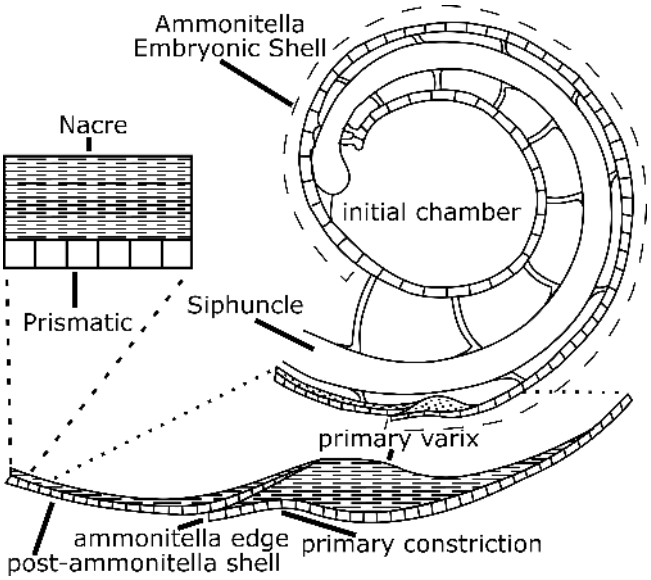

Figure 7. Diagram of the exterior and cross section of the early whorls of an ammonite, modified from (Landman et al. 1996). Ammonitella (embryonic shell) comprises the initial chamber and shell wall up to the primary constriction. This portion of the shell has prismatic microstructure. The primary varix consists of nacre and is hypothesized to have precipitated at or close to hatching (Landman et al. 1996). All shell precipitated after the primary varix comprises a thin outer prismatic layer and a thicker nacreous layer (Kulicki 1996). Septa are thought to precipitate in the ammonitella later, after hatching as additional shell grows (Landman et al. 1996).

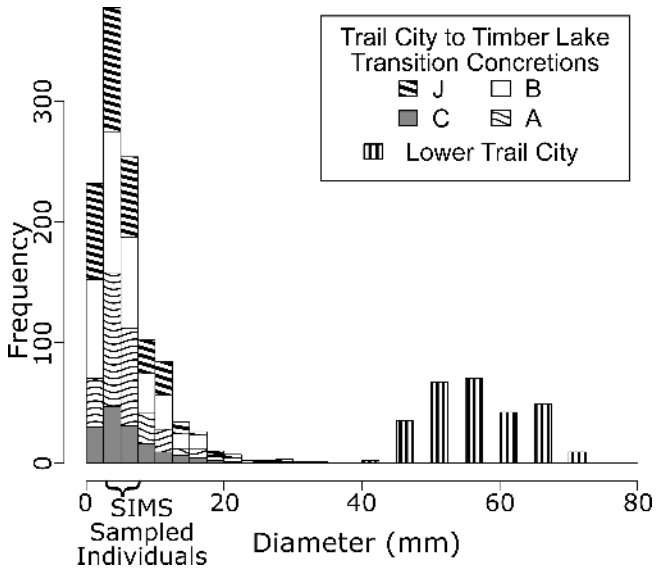

Figure 8. Histogram showing the size distribution of scaphite ammonites in four *abyssinus* or transition concretions from the transition zone between the Trail City Member and Timber Lake Member and sixteen additional concretions from the Trail City Member in the Fox Hills Formation, Dewey County, South Dakota (Data from Landman et al., 2008). The J concretion that contains the individuals sampled in this study has a similar distribution of sizes to other transition concretions (A, B, and C). The diameter of the five *Hoploscaphites comprimus* analyzed in this study ranges from 2.9 to 7.8 mm, encompassing the mean and modal diameter of juveniles from these concretions. Trail City ammonite diameters are from concretions of the Limopsis-Gervillia Assemblage Zone and are much larger and contain no juveniles (Landman et al. 2008).

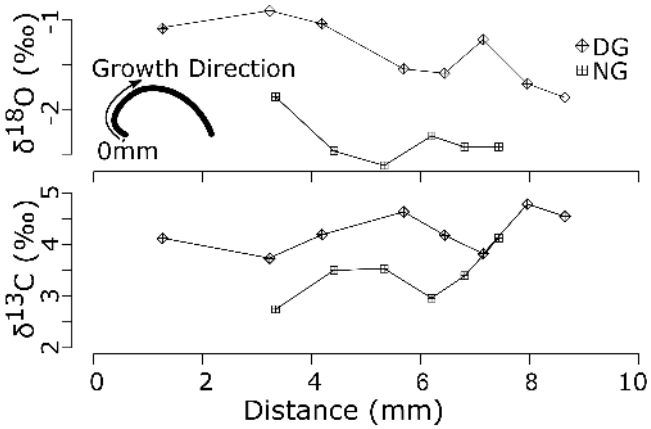

Figure 9. Oxygen and carbon isotope values from two micromilled Protocardia bivalves. Simple diagram inset shows the growth direction away from the umbo of the bivalves and orienting the zero position of the growth distance axis. Line plots showing the $\delta^{18}O_{AragCal}$ and $\delta^{13}C_{AragCal}$ of micromilled calcite from each bivalve. Partial sinusoids may indicate some seasonal variability. The range between individuals may indicate transport from near shore. Analysis precision is 0.07‰ (2 sd) for $\delta^{18}O$ and 0.16 ‰ (2 sd) for $\delta^{13}C$.

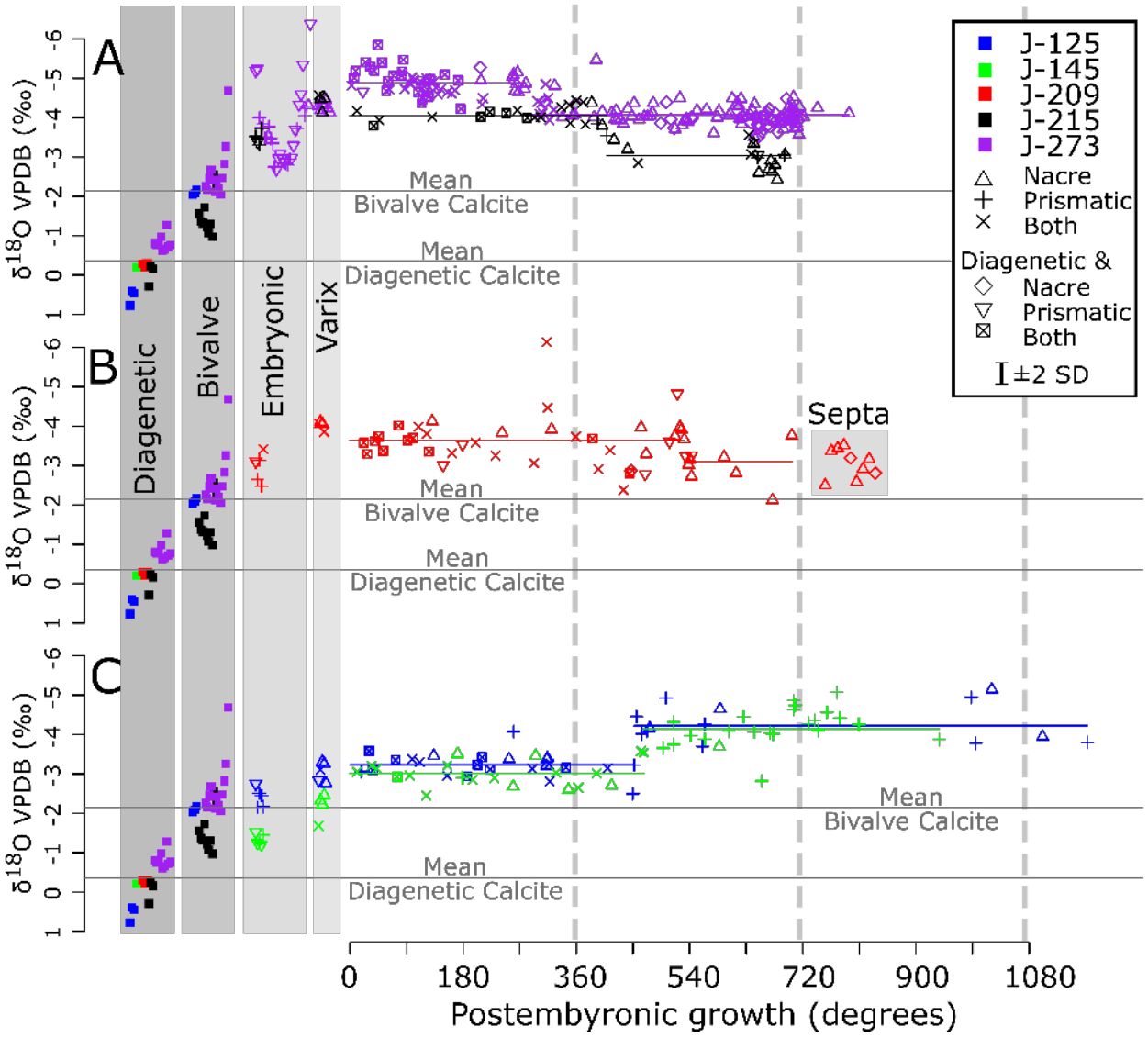

Figure 10. Comparison of ~10 µm SIMS analyses of $\delta^{18}O$ from diagenetic calcite, bivalve calcite, and ammonite aragonite plotted against whorl number (degrees). Ammonites are divided into three groups to facilitate discussion (A, black-J-273 and purple-J-215; B, red-J-209; and C, green-J-125 and blue-J-145). The distribution of SIMS measured diagenetic and bivalve calcite is reproduced to compare to all three ammonite datasets. Microstructure measured by SIMS of post-varix shell is indicated by different symbols. Changing means through the timeseries were identified using the changepoint package in R (Killick and Eckley 2014). A shift in mean $\delta^{18}O$ was identified in all five individuals between 270° and 540°. Means for the identified segments of the datasets are plotted corresponding to sample colors.

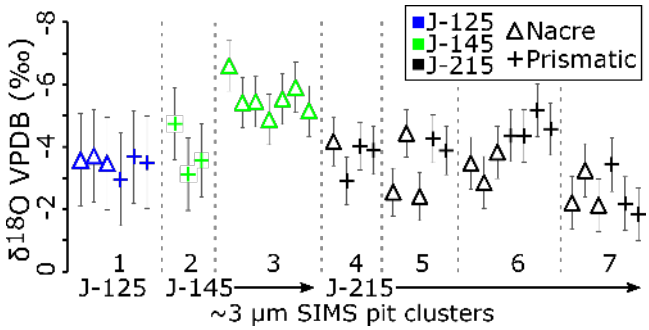

Figure 11. Comparison of $\delta^{18}O$ from ~3 µm SIMS pits on nacre and prismatic layers of J-215, J-145, and J-125. Grey dashed vertical lines demarcate clusters of pits that are closely adjacent (within ~20 µm) to each other. Cluster 5 may suggest differences between the two microstructures, however any apparent difference here could be due to difference in the timing of precipitation between the two locations. Overall, there is no detectable, systematic difference in $\delta^{18}O$ that corresponds to differing microstructures of the ammonite shell, given the larger instrumental precision (~0.7 ‰ 2SD). Larger analysis spots (~10 µm) with smaller error (~0.3‰ 2SD) do not show a systematic difference between the microstructures either (Fig. 10).

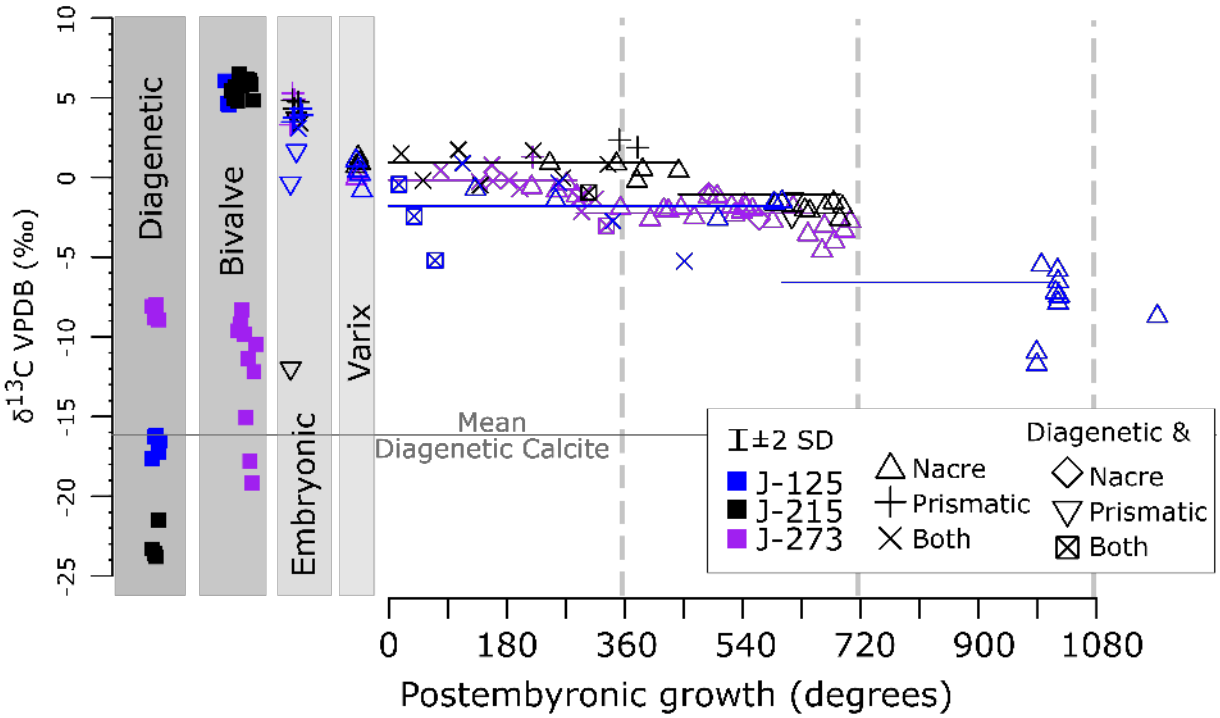

Figure 12. Comparison of $\delta^{13}C$ SIMS analyses from diagenetic calcite, bivalve calcite, and ammonite aragonite plotted against whorl number (degrees) for J-125, J-215, and J-273. Infilling diagenetic calcite has $\delta^{13}C$ that is much more negative than the ammonite shells. Each diagenetic infilling has a distinct $\delta^{13}C$ value, that may indicate lower $\delta^{13}C$ of the organic carbon bicarbonate source. The diagenetic calcite has lower $\delta^{13}C_{AragCal}$ (-23‰ to -8.4‰), which may indicate remineralized organic matter. Embryonic shell has the most positive values measured ~5‰ (VPDB). These values change to 0‰ (VPDB) in the varix. This large change could be due to different $\delta^{13}C$ of diet or dissolved inorganic carbon (DIC) from vertical movement in a water column that has a freshwater lens.

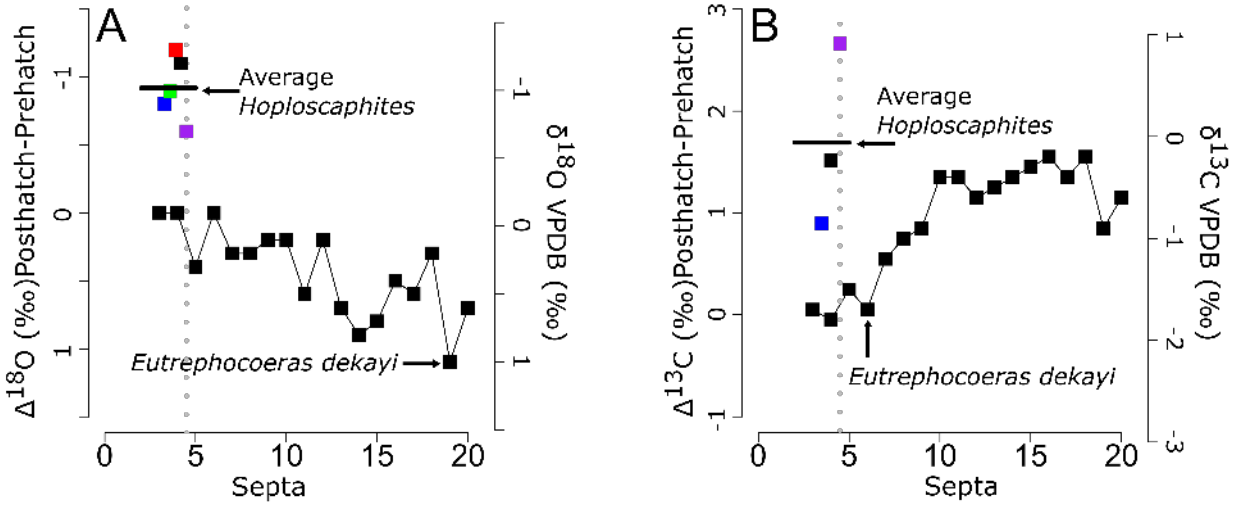

Figure 13. Septa number vs $\delta^{18}O$ and $\delta^{13}C$ from a *Eutrephoceras dekayi* collected in the Fox Hills formation compared to the pre-to-post hatching change in the scaphites measured in this study. *Eutrephoceras dekayi* data are from sample FH1 (Landman et al. 1983). A and B Hatching is inferred to have occurred between septa 4 and 5 and is indicated by the dashed vertical grey line. The right axis of both A and B show the $\delta^{18}O$ and $\delta^{13}C$ values as reported in (Landman et al. 1983). The left axis shows the change in $\delta^{18}O$ and $\delta^{13}C$ from the average pre-hatching values (septa 3 and 4). Points scattered around the average *Hoploscaphites* line indicate the average varix isotope ratio minus the average embryonic isotope ratio for each ammonite. In A, from left to right points are J-125, J-145, J-209, J-215, and J-273. In B, from left to right points are J-145, J-215, and J-273. The average embryonic to varix change is approximately -1‰ for $\delta^{18}O$ and +1.9‰ for $\delta^{13}C$. The ammonites in this study clearly show habitat change at hatching that this *Eutrephoceras dekayi* did not undergo (compare to Figs. 8 and 10).

Table 1. Count of varices in in five specimens of *Hoploscaphites comprimus*, Concretion J, Fox Hills Formation, Dewey County, South Dakota.

Sample	# of Pathological varix	Description
J-125	6	Mostly short
J-145	5, maybe 6?	Mostly short
J-209	4, maybe 5?	Mostly short
J-215	2, maybe 5?	Mostly long and flat
J-273	1, maybe 2?	Mostly long and flat

Table 2. Summary of SIMS measured $\delta^{18}O$ values from 10 µm spots and temperatures calculated assuming aragonite precipitated in equilibrium with seawater at different values of $\delta^{18}O$. Temperature calculations were done with the equation derived by Kim et al. (2007b).

Sample	**Whorl**	**Mean $\delta^{18}O$** VPDB (‰)	**sd $\delta^{18}O$**	**Number of analyses**	**Temp (°C)** $\delta^{18}O_{SW}$ -1‰ VSMOW	**Temp (°C)** $\delta^{18}O_{SW}$ -2‰ VSMOW	**Temp (°C)** $\delta^{18}O_{SW}$ -3‰ VSMOW
J-125	E	-2.4	0.3	5	22.2	17.4	12.7
	V	-3.1	0.2	5	25.7	20.8	16.1
	0-0.5	-3.3	0.2	8	26.6	21.7	16.9
	0.5-1	-3.3	0.3	13	26.6	21.7	16.9
	1-1.5	-3.8	0.8	8	29.4	24.4	19.5
	1.5-2	-4.2	0.5	3	31.5	26.4	21.5
	2-2.5	-	-	0	-	-	-
	2.5-3	-4.6	0.7	3	33.8	28.6	23.6
	3-3.5	-3.9	0.1	2	29.7	24.7	19.8
J-145	E	-1.3	0.1	5	16.9	12.3	7.8
	V	-2.2	0.3	4	21.0	16.3	11.7
	0-0.5	-3.0	0.3	9	25.4	20.5	15.8
	0.5-1	-2.9	0.3	6	24.8	19.9	15.2
	1-1.5	-3.4	0.6	8	27.3	22.3	17.5
	1.5-2	-4.1	0.5	12	31.0	25.9	21.0
	2-2.5	-4.4	0.3	7	32.8	27.6	22.6
	2.5-3	-3.9	-	1	29.8	24.7	19.8
J-209	E	-3.0	0.4	5	25.0	20.1	15.3
	V	-4.0	0.1	4	30.5	25.5	20.6
	0-0.5	-3.6	0.3	15	28.3	23.4	18.5
	0.5-1	-4.0	1.0	8	30.4	25.4	20.5
	1-1.5	-3.4	0.6	18	27.5	22.5	17.7
	1.5-2	-3.0	0.5	7	25.2	20.3	15.6
	Septa	-3.1	0.4	9	25.5	20.6	15.8
J-215	E	-3.4	0.2	5	27.4	22.4	17.6
	V	-4.4	0.2	4	32.7	27.5	22.6
	0-0.5	-4.0	0.2	4	30.3	25.3	20.4
	0.5-1	-4.1	0.2	11	31.1	26.0	21.1
	1-1.5	-3.7	0.5	9	28.8	23.8	19.0
	1.5-2	-3.0	0.3	14	25.1	20.2	15.4
J-273	E	-3.8	0.9	30	29.1	24.1	19.2
	V	-4.3	0.1	7	32.0	26.8	21.9
	0-0.5	-4.9	0.3	42	35.3	30.0	25.0
	0.5-1	-4.6	0.4	27	33.5	28.3	23.3
	1-1.5	-4.1	0.3	29	30.9	25.8	20.9
	1.5-2	-4.0	0.2	71	30.5	25.4	20.5
	2-2.5	-4.1	0.1	3	31.1	26.0	21.1